FINITE ELEMENT MODELING OF HUMAN ARTERY TISSUE WITH A NONLINEAR MULTI-MECHANISM INELASTIC MATERIAL

by

Sergey Sidorov

B.S., Saint-Petersburg State Polytechnical University, 2001

M.S., Saint-Petersburg State Polytechnical University, 2003

Submitted to the Graduate Faculty of

School of Engineering in partial fulfillment

of the requirements for the degree of

Doctor of Philosophy

University of Pittsburgh

2007

UNIVERSITY OF PITTSBURGH

SCHOOL OF ENGINEERING

This dissertation was presented

by

Sergey Sidorov

It was defended on

March 15, 2007

and approved by

Anne M. Robertson, Associate Professor, Mechanical Engineering and Materials Science Dept.

Roy D. Marangoni, Associate Professor, Mechanical Engineering and Materials Science Dept.

William S. Slaughter, Associate Professor, Mechanical Engineering and Materials Science Dept.

Dissertation Director: Michael R. Lovell, Associate Professor, Industrial Engineering Dept.

FINITE ELEMENT MODELING OF ANEURYSM DEVELOPMENT AND GROWTH WITH A NONLINEAR MULTI-MECHANISM INELASTIC MATERIAL

Sergey Sidorov, PhD

University of Pittsburgh, 2007

Due to limited experimental data and a lack of understanding of the underlying microstructural deformation mechanisms involved, modeling of material behavior of biomechanical tissues presents a rather formidable task. In this dissertation, a nonlinear multi-mechanism inelastic material model is formulated for modeling vascular tissue, collagen recruitment and elastin degradation. The model is implemented into the commercial finite element software package ANSYS with user programmable features. Although the idea of using several deformation mechanisms in the same material model is by no means novel, it is the first time such model is being implemented in a commercial finite element package and applied to a numerical study of physiological processes taking place inside the vascular walls. Two numerical examples are presented: a simulation of angioplasty procedure, and a finite element analysis of fusiform aneurysm development and growth. This is by far not the exhaustive list of possible applications of the developed material model; implementation in a commercial finite element code will help facilitate innovative developments, including new ways to surgically treat vascular disorders.

TABLE OF CONTENTS

LIST OF TABLES

LIST OF FIGURES

ACKNOWLEDGEMENTS

I would like to take this opportunity to express my immense gratitude to everyone who has given me their invaluable support and assistance during my apprenticeship at the University of Pittsburgh.

I would like to express my deepest gratitude to my advisor, Dr. Michael Lovell, for his invaluable guidance, caring, and providing me with an excellent atmosphere for doing research. I would like to thank Dr. Guoyu Lin, for being a patient mentor and a perpetual source of knowledge and information. I would also like to thank all the other employees of Ansys, Inc., for all their help, and for accepting me as a fully-fledged member of their team.

I would like to express my appreciation to the members of my committee — Dr. Roy Marangoni, Dr. William Slaughter — for taking their time to attend my PhD defense.

Special thanks to Glinda Harvey for all her help, encouragement and friendship.

My heartfelt gratitude to those graduate students of the Department of Mechanical Engineering whom I had an honor of calling “friends”: Roxana Cisloiu, Pushkarraj Deshmukh, Khaled Bataineh, Ventzi Karaivanov, Sandeep Urankar.

1.0 INTRODUCTION

The current work was inspired by a desire to study mechanisms leading to formation of aneurysms, as well as to assist in development of surgical treatment of the aforementioned disease. An aneurysm is a localized dilation of a blood vessel. Aneurysms are most commonly found in arteries in or near the Circle of Willis (intracranial aneurysms – ICA), and in the aorta (aortic aneurysms). Intracranial aneurysms occur in up to 6% of the population and have an average maximum diameter of 10 mm [1]. The overall annual risk of rupture for ICAs was found to be 1.9%. Abdominal aortic aneurysms (AAA) occur in 3% – 9% of the population, causing 15,000 deaths per year only in the United States [2, 3]. The surgery on an AAA is performed whenever its dimension exceeds 50 mm [4 – 6].

Depending on their geometry we can distinguish between saccular and fusiform aneurysms (Figure 1). Most intracranial aneurysms are saccular in nature, whereas the majority of aortic aneurysms are fusiform. Fusiform aneurysms manifest themselves by pressing on surrounding tissue; saccular aneurysms are usually asymptomatic until rupture, which causes spontaneous subarachnoid hemorrhage (SAH). SAH results in death in 35 – 50 % of the patients [7].

In order to gain some insight into the micromechanical processes leading to the initiation of aneurysms, it is important to understand the morphological structure of the arterial wall (Figure 2).

Arteries are generally distinguished as *elastic* (arteries adjacent to the heart) or muscular. Elastic arteries usually have larger diameters, whereas muscular arteries are smaller vessels.

Arteries of either type consist of three layers (Figure 2): the tunica *intima*, tunica *media* and tunica *adventitia* [7].

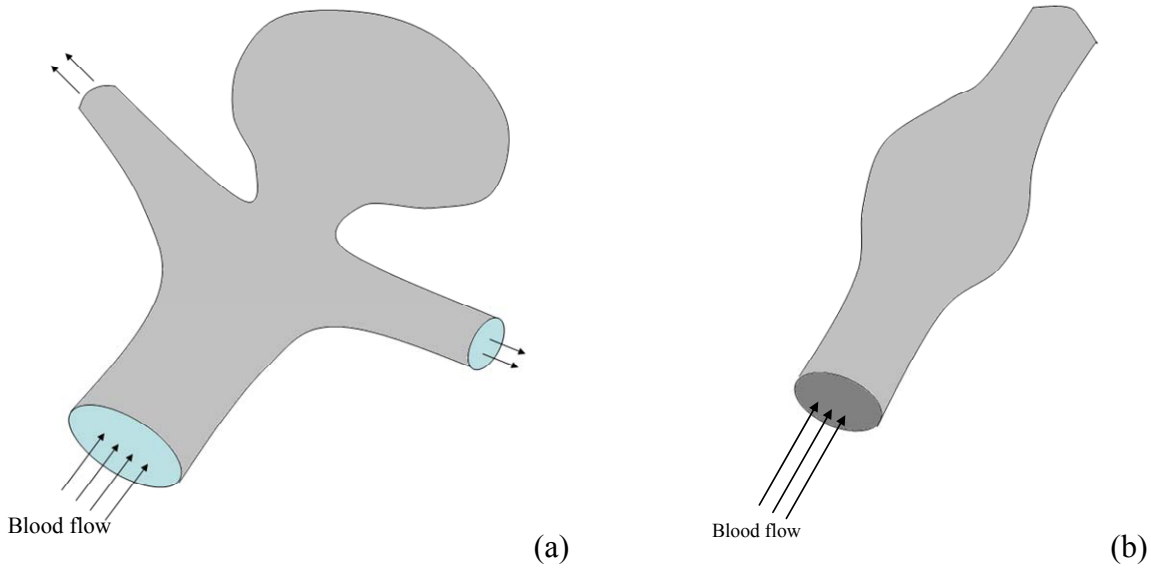

Figure 1. Aneurysms: (a) saccular, (b) fusiform

The intima is the innermost layer of the artery. It consists of a layer of endothelial cells and a thin basal membrane [7]. Intima is known to contribute very little to the solid mechanical response of the arterial tissue [8].

The media is the middle layer of the artery. It is composed of a plexus of smooth muscle cells, as well as the elastin and collagen fibers. From the mechanical point of view the media is the most important layer of the arterial wall.

The adventitia is the outermost layer of the arterial wall, consisting of a maze of collagen fibers combined with elastin, nerves, fibroblasts (cells that supply collagen) and the vasa vasorum (the network of small vessels that provide cells that make up the outer wall of the

artery). At low pressure levels tunica adventitia is more compliant than tunica media. As the load increases, however, the tunica adventitia becomes a stiff shell, restraining the artery from excessive deformation and damage.

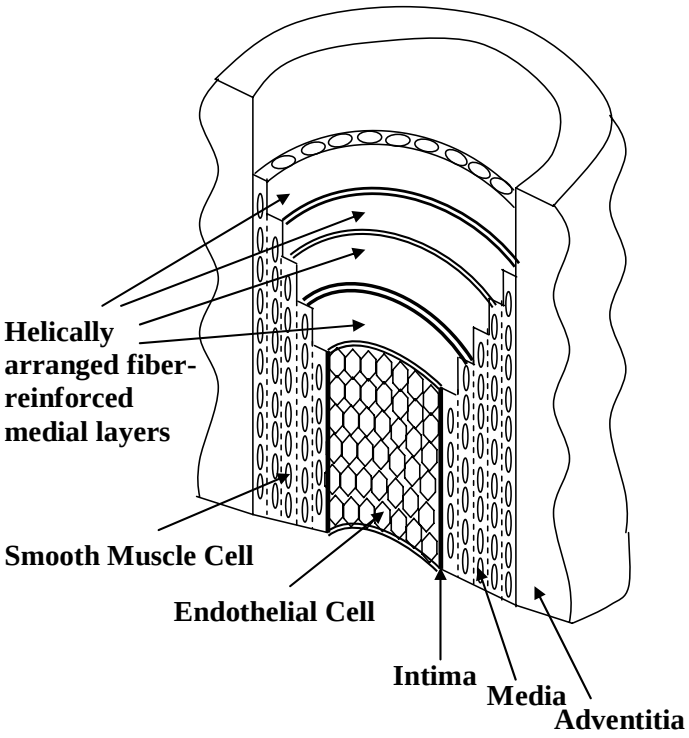

Figure 2. Histological structure of a healthy artery

There has been few publications on mechanical properties of blood vessels and aneurysms, as well as about the possible causes of the disease. A very important paper was published in 1972 by Scott et al [9]. Although it is over 30 years old, this paper contains experimental data that "appears to be the best available on human lesions" [7]. Their research focused on cyclic pressure inflation experiments on cerebral arteries. The tension (product of radius and pressure) vs. radius data obtained by Scott's group is presented in Figure 3. An interesting phenomenon discovered by Scott et al is that the tension vs. radius data obtained in

first three loading runs is fundamentally different from the second set of curves obtained from runs four through nine. This allowed conjecture that some drastic microstructural change occurred within the arterial wall, namely that elastin contained in the arterial wall ruptured. Scott et al. [9] claimed that rupture of elastin is the major cause of the aneurysm initiation. This is consistent with the histological evidence [c.f. 10], which shows that elastin within the aneurysm tissue is decreased and fragmented.

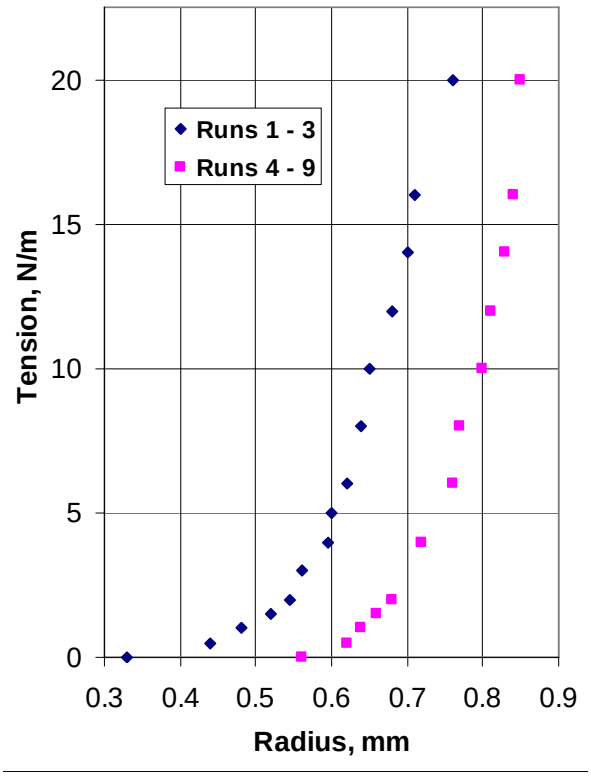

Figure 3. Tension vs. radius data from an anterior cerebral artery, reproduced from Figure 5B in [9]

Similar results were obtained for aortic aneurysms. Drangova et al [11] used a computer tomography scanner for in vitro studies of arterial geometry and elastic properties of the abdominal aortic aneurysms. They have found a "sixfold decrease in elastin content in the aneurysm, compared to the normal aorta."

Traditionally soft tissues are modeled with hyperelastic materials. Hyperelastic materials are characterized by a specific form of a *strain energy density function* [12]. Mathematical expressions for different forms of strain energy density functions for various hyperelastic materials are provided in Appendix B.

Several publications on numerical modeling of soft tissues are to be found [13 – 15, 17, 21 – 23]. Bellamy et al. [13] used a Mooney-Rivlin hyperelastic material model to analyze facial prostheses. Büchler et al. [14] employed an exponential hyperelastic material to model muscle tissue, and a Neo-Hookean hyperelastic material to model cartilage in their research study of mechanical behavior of a human shoulder. Cheung et al. [15] utilized a polynomial hyperelastic material in their analysis of the foot during standing. All these researchers used the commercial FE software package ABAQUS [16]. Some studies apply anisotropic materials to numerically investigate mechanical response of soft tissues (c.f. [17]). These material models are also available in commercial finite element packages, such as ANSYS [18] (which utilizes a formulation by Kaliske [19]) or LS-DYNA [20] (which utilizes a formulation by Weiss et al. [21]). LS-DYNA also features two very specific material models MAT_HEART_TISSUE (based on a theoretical work of Guccione et al. [22]) and MAT_LUNG_TISSUE (based on a theoretical work done by Vawter [23]).

Commercial finite element packages provide very convenient tools for working with hyperelastic materials. Most of them feature so-called curve-fitting capabilities, which allow users to choose the material model most suitable to their needs, as well as calculate material parameters.

Very few attempts of mathematical modeling of mechanical behavior aneurysms have been published. Most studies view aneurysms as a separate entity from the vascular tissue from

which they had evolved, thus leaving the process of aneurysm development outside the scope of the research. An important theory was proposed by Humphrey and Rajagopal [24]. They developed the so-called "growth and remodeling" of collagen theory. Wulandana and Robertson [25] formulated a new mathematical model to describe the initiation of an aneurysm from a healthy arterial tissue. Their research addressed modeling the important phenomena of elastin rupture and collagen recruitment.

The material model, developed in [25], is termed a "dual-mechanism" model due to its separate treatment of mechanical response of elastin and collagen fibers. The idea of using more than one deformation mechanism in the same material model is not novel (c.f. [26]); Wulandana [27] was the first to apply a multi-mechanism model to study mechanical behavior of human arteries. Nevertheless, such models have never been implemented in a commercial finite element package.

We shall hereby adopt the approach of [25], and formulate a computational model that we incorporate into the commercial code ANSYS. The formulation that we offer in this dissertation is somewhat different form the formulation of Wulandana and Robertson [25] in a sense that unlike in [25] we model the tissue as a compressible material. The main reason why we chose to model our material as compressible is the fact that the user defined material feature of ANSYS is only suitable for modeling compressible materials. There are, however, other arguments in favor of a compressible model. Traditionally, the arterial wall is considered incompressible, although the experimental evidence supporting the incompressibility assumption is incomplete [28]. Furthermore, Boutouyrie et al [29] claim that volumetric effects play a significant part in deformation of carotid arteries. Chuong and Fung [30] argue that the

incompressibility assumption is in contradiction with the fact that fluid can move across the vessel wall due to intraluminal pressure or shear stress.

We are hoping that the model that we propose will allow us to shed some light on whether or not incompressibility effects play an important role in the mechanical response of the arterial tissue. Setting the compressibility parameter (see Section 2.1) to a very small value renders the model *nearly incompressible*, and thus the mechanical response becomes the same as that of an incompressible model. In other words, when the compressibility parameter is sufficiently small, the mechanical response of our material becomes identical to that of the material of [25].

The remainder of this dissertation will proceed as follows. In Chapter 2, a brief mathematical description of the material model will be given (derivation of some tensor algebra results are left for Appendix A). Chapter 3 discusses the testing of the finite element code. Chapters 4 and 5 will describe two numerical examples, illustrating how the developed material model can be applied to the numerical study of physiological processes taking place within the arterial wall, as well as some surgical procedures performed on human arteries. Although the material model was developed as an attempt to study biomechanical behavior of aneurysms, Chapter 4 demonstrates that the model can serve other purposes as well, namely the simulation of balloon angioplasty procedures. Finally, the conclusions of this dissertation are provided in Chapter 6.

2.0 MATHEMATICAL MODEL

The two passive load bearing components of the arterial wall are elastin and collagen fibers [25]. The mechanical contribution of the rest of the constituents of the arterial tissue is insignificant, and, therefore, can be excluded from consideration. Wulandana and Robertson [25] proposed a structurally motivated phenomenological model of the arterial wall deformation that is illustrated in Figure 4.

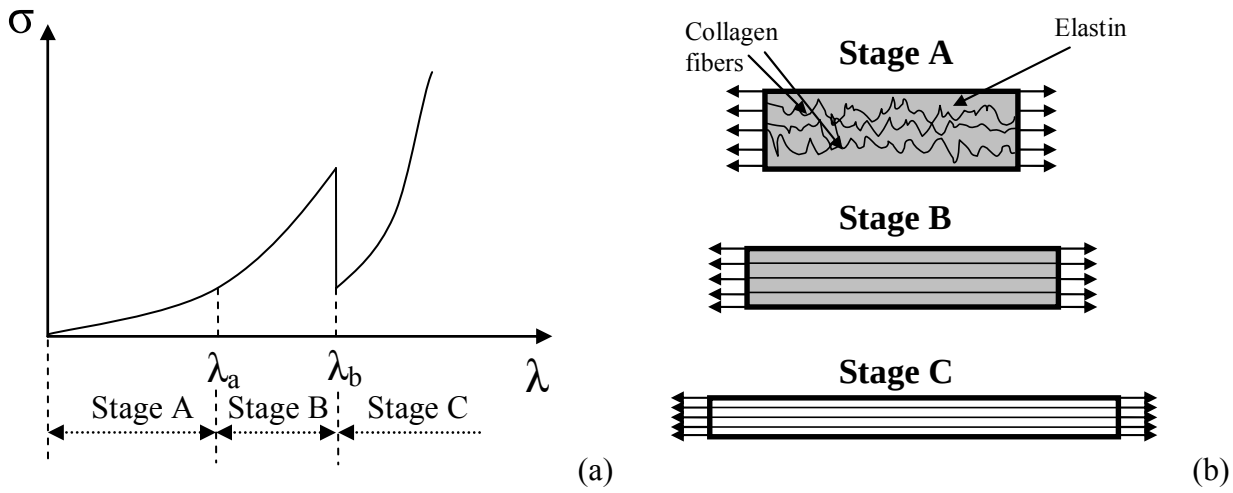

Figure 4. Stages of arterial tissue deformation

Figure 4 (a) shows a stress-stretch curve pertaining to a uniaxial tension of a vascular tissue material sample. Figure 4 (b) is a schematic illustrating microstructural changes occurring within the sample. At low loads in healthy vessels collagen fibers are crimped [8], and thus elastin is the sole load bearing component (Stage A in Figure 4). Then, as stretch exceeds a

certain value – referred to as λ_a – the collagen fibers begin to bear load (collagen recruitment – Stage B in Figure 4); thus, as we continue deforming the sample, two deformation mechanisms corresponding to elastin and collagen are present. As stretch reaches another material specific value denoted as λ_b, elastin ruptures. This corresponds to a sudden decrease of stress in the sample (Figure 4 (a)). As we continue to load the specimen, stress increases, but only the collagen deformation mechanism is active (Stage C in Figure 4). Note that after the elastin rupture, the unloaded configuration changes. If we unload the specimen from Stage C, the stress-stretch curve will cross the horizontal axis at a point different from the origin.

2.1 CONTINUUM MECHANICS FORMULATION

Utilizing the phenomenological model of mechanical behavior of vascular tissue outlined above as a basis, we will now develop the continuum mechanics framework necessary for implementing the material model into a finite element software package. The formulation that we offer is based on the theory of Wulandana and Robertson [25].

Notation, utilized in this section, is discussed in Appendix D.

Let us consider a three-dimensional body Ω. As described by Wulandana and Robertson, let us define two reference configurations κ_1 and κ_2 (Figure 5), corresponding to the initial unloaded state and the state when collagen fibers begin to bear load respectively; κ_2 is the unloaded configuration for collagen.

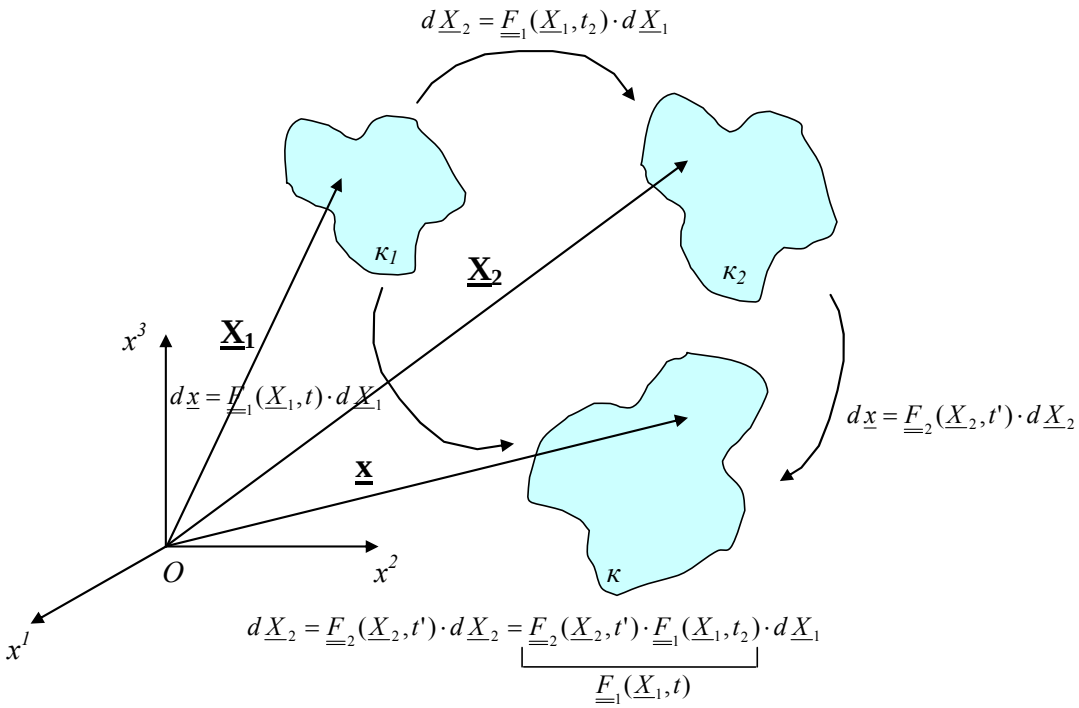

Figure 5. Different reference configurations for the multi-mechanism model

A generic particle Y of the body Ω can be identified by a vector $\underline{X}_1$ in reference configuration κ_1, or by a vector $\underline{X}_2$ in reference configuration κ_2. The motion of the particle Y can be described by

$$\underline{x} = \underline{\varphi}_{\kappa_1}(\underline{X}_1, t), \tag{1}$$

where $\underline{\varphi}_{\kappa_1} : \Omega \times R \to R^3$.

If κ_2 is achieved at time $t=t_2$, $\underline{X}_2 = \underline{\varphi}_{\kappa_1}(\underline{X}_1, t_2)$. Relative to configuration κ_2 the motion of the particle Y may thus be described as

$$\underline{x} = \underline{\varphi}_{\kappa_2}(\underline{X}_2, t), \tag{2}$$

where $\underline{\varphi}_{\kappa_2} : \Omega \times R \to R^3$.

The deformation gradient for the particle Y at time t relative to the reference configurations κ_1 and κ_2 can now be defined as

$$\underline{\underline{F}}_1(t) = \frac{\partial \underline{\varphi}_{\kappa_1}(\underline{X}_1, t)}{\partial \underline{X}_1}, \tag{3}$$

and

$$\underline{\underline{F}}_2(t) = \frac{\partial \underline{\varphi}_{\kappa_2}(\underline{X}_2, t)}{\partial \underline{X}_2} \tag{4}$$

respectively.

Clearly,

$$\underline{\underline{F}}_2(t) = \underline{\underline{F}}_1(t) \cdot \underline{\underline{F}}_1^{-1}(t_2). \tag{5}$$

The right Cauchy-Green deformation tensor for the particle Y at time t relative to the reference configurations κ_1 and κ_2 can now be defined as

$$\underline{\underline{C}}_1 = \underline{\underline{F}}_1^T \cdot \underline{\underline{F}}_1, \tag{6}$$

and

$$\underline{\underline{C}}_2 = \underline{\underline{F}}_2^T \cdot \underline{\underline{F}}_2 \tag{7}$$

respectively, where dependency on time t is omitted.

We assume that the material is quasi-hyperelastic, and that there exists a *strain energy density function* Ψ (also known as the *elastic potential*) from which the stress can be derived for each point $\underline{X}$. Ψ is a function of the right Cauchy-Green deformation tensor (or its invariants).

Following Simo and Hughes [31] we split the strain energy density function into volumetric and isochoric parts

$$\Psi = \Psi_{vol} + \Psi_{iso}, \tag{8}$$

and define the modified deformation gradients and right Cauchy-Green deformation tensors relative to reference configurations κ_1 and κ_2 according to

$$\underline{\underline{F}}_1 = J_1^{1/3}\overline{\underline{\underline{F}}}_1 \text{ and } \underline{\underline{F}}_2 = J_2^{1/3}\overline{\underline{\underline{F}}}_2, \qquad (9)-(10)$$

and

$$\underline{\underline{C}}_1 = J_1^{2/3}\overline{\underline{\underline{C}}}_1 \text{ and } \underline{\underline{C}}_2 = J_2^{2/3}\overline{\underline{\underline{C}}}_2, \qquad (11)-(12)$$

where

$$J_\alpha = \det \underline{\underline{F}}_\alpha, \alpha = 1,2. \qquad (13)$$

The volumetric part is assumed to have a simple form

$$\Psi_{vol} = \frac{1}{d}(J_1 - 1)^2, \qquad (14)$$

where d is called the *incompressibility parameter*.

As in [25], we can define the deformation parameter

$$s = \hat{s}(\overline{\underline{\underline{C}}}_1), \qquad (15)$$

a scalar function of the deformation gradient. The value which the deformation parameter takes at time $t=t_2$ is denoted as s_a. Following the work of [25], we assume

$$s = tr\overline{\underline{\underline{C}}}_1 - 3. \qquad (16)$$

Taking into account the above considerations (Section 2), we choose the following form for the isochoric part of the strain energy density function

$$\Psi_{iso} = \begin{cases} \Psi_1(\bar{I}_1^{(1)}), & 0 \le s \le s_a \\ \Psi_1(\bar{I}_1^{(1)}) + \Psi_2(\bar{I}_1^{(2)}), & s_a \le s \le s_b \\ \Psi_2(\bar{I}_1^{(2)}), & s \ge s_b \end{cases}, \qquad (17)$$

where

$$\bar{I}_1^{(1)} = tr\overline{\underline{\underline{C}}}_1, \quad \bar{I}_1^{(2)} = tr\overline{\underline{\underline{C}}}_2, \qquad (18)-(19)$$

and s_b is the value the deformation parameter s assumes at the moment of elastin breakage.

As outlined in [25], we can assume the strain energy density function to take the exponential form:

$$\Psi_1(\bar{I}_1) = \frac{\alpha_1}{2\gamma_1}(e^{\gamma_1(\bar{I}_1-3)} - 1) \tag{20}$$

and

$$\Psi_2(\bar{I}_2) = \frac{\alpha_2}{2\gamma_2}(e^{\gamma_2(\bar{I}_2-3)} - 1)\,. \tag{21}$$

Further we split the second Piola-Kirchhoff stress tensor into volumetric and isochoric part as

$$\underline{\underline{S}} = \underline{\underline{S}}_{vol} + \underline{\underline{S}}_{iso}\,. \tag{22}$$

The volumetric part is defined as

$$\underline{\underline{S}}_{vol} = 2\frac{\partial \Psi_{vol}(J_1)}{\partial \underline{\underline{C}}_1} = 2\left[\frac{\partial \Psi_{vol}}{\partial J_1}\frac{\partial J_1}{\partial \underline{\underline{C}}_1}\right] = J_1 p \underline{\underline{C}}_1^{-1}, \tag{23}$$

where

$$p = \frac{\partial \Psi_{vol}(J_1)}{\partial J_1} = \frac{2}{d}(J_1 - 1)\,. \tag{24}$$

We define the isochoric part of the second Piola-Kirchhoff stress tensor as follows

$$\underline{\underline{S}}_{iso} = \begin{cases} 2\dfrac{\partial \Psi_1(\bar{\underline{\underline{C}}}_1)}{\partial \underline{\underline{C}}_1}, & 0 \le s \le s_a \\ 2\dfrac{\partial \Psi_1(\bar{\underline{\underline{C}}}_1)}{\partial \underline{\underline{C}}_1} + 2\dfrac{\partial \Psi_2(\bar{\underline{\underline{C}}}_2)}{\partial \underline{\underline{C}}_2}, & s_a \le s \le s_b \\ 2\dfrac{\partial \Psi_2(\bar{\underline{\underline{C}}}_2)}{\partial \underline{\underline{C}}_2}, & s \ge s_b \end{cases} = \begin{cases} \underline{\underline{S}}_1, & 0 \le s \le s_a \\ \underline{\underline{S}}_1 + \underline{\underline{S}}_2, & s_a \le s \le s_b \\ \underline{\underline{S}}_2, & s \ge s_b \end{cases}. \tag{25}$$

Taking derivatives and using chain rule we obtain for $\underline{\underline{S}}_1$

$$\underline{\underline{S}}_1 = 2\frac{\partial \Psi_1(\underline{\underline{\bar{C}}}_1)}{\partial \underline{\underline{C}}_1} = 2\left[\frac{\partial \Psi_1(\underline{\underline{\bar{C}}}_1)}{\partial \underline{\underline{\bar{C}}}_1} : \frac{\partial \underline{\underline{\bar{C}}}_1}{\partial \underline{\underline{C}}_1}\right] = J^{-2/3}\,\underline{\underline{\underline{\underline{P}}}}_1 : \underline{\underline{\bar{S}}}(\underline{\underline{\bar{C}}}_1), \tag{26}$$

where $\underline{\underline{\underline{\underline{P}}}}_1$ is a *projection tensor* (see Appendix A), and

$$\underline{\underline{\bar{S}}}_1 = 2\frac{\partial}{\partial \underline{\underline{\bar{C}}}_1}\Psi_1(\underline{\underline{\bar{C}}}_1) = \alpha_1 e^{\gamma_1(\bar{I}_1-3)}\underline{\underline{I}} \tag{27}$$

($\underline{\underline{I}}$ is a second order unit tensor).

Similarly for $\underline{\underline{S}}_2$

$$\underline{\underline{S}}_2 = 2\frac{\partial \Psi_2(\underline{\underline{\bar{C}}}_2)}{\partial \underline{\underline{C}}_2} = 2\left[\frac{\partial \Psi_1(\underline{\underline{\bar{C}}}_2)}{\partial \underline{\underline{\bar{C}}}_2} : \frac{\partial \underline{\underline{\bar{C}}}_2}{\partial \underline{\underline{C}}_2}\right] = J_2^{-2/3}\,\underline{\underline{\underline{\underline{P}}}}_2 : \underline{\underline{\bar{S}}}_2(\underline{\underline{\bar{C}}}_2), \tag{28}$$

where $\underline{\underline{\underline{\underline{P}}}}_2$ is a *projection tensor* (see Appendix A), and

$$\underline{\underline{\bar{S}}}_2 = 2\frac{\partial}{\partial \underline{\underline{\bar{C}}}_2}\Psi_2(\underline{\underline{\bar{C}}}_2) = \alpha_2 e^{\gamma_2(\bar{I}_2-3)}\underline{\underline{I}}\,. \tag{29}$$

Analogously the elasticity tensor is split into volumetric and isochoric parts.

$$\underline{\underline{\underline{\underline{C}}}} = \underline{\underline{\underline{\underline{C}}}}_{vol} + \underline{\underline{\underline{\underline{C}}}}_{iso}\,. \tag{30}$$

For $\underline{\underline{\underline{\underline{C}}}}_{vol}$ we have

$$\underline{\underline{\underline{\underline{C}}}}_{vol} = 2\frac{\partial \underline{\underline{S}}_{vol}}{\partial \underline{\underline{C}}_1} = J_1\tilde{p}\,\underline{\underline{C}}_1^{-1} \otimes \underline{\underline{C}}_1^{-1} - 2J_1 p\,\underline{\underline{C}}_1^{-1} \oplus \underline{\underline{C}}_1^{-1}, \tag{31}$$

where $\tilde{p} = p + p\frac{\partial p}{\partial J_1}$. For derivation of (31), and the explanation of the symbol "$\oplus$", please refer to Appendix A.

The isochoric part of the elasticity tensor is defined as follows

$$
{}^{4}\underset{=}{\underset{=}{C}}_{iso} = \begin{cases} 2\dfrac{\partial \underset{=}{S}_1(\overline{\underset{=}{C}}_1)}{\partial \underset{=}{C}_1}, & 0 \le s \le s_a \\ 2\dfrac{\partial \underset{=}{S}_1(\overline{\underset{=}{C}}_1)}{\partial \underset{=}{C}_1} + 2\dfrac{\partial \underset{=}{S}_2(\overline{\underset{=}{C}}_2)}{\partial \underset{=}{C}_2}, & s_a \le s \le s_b \\ 2\dfrac{\partial \underset{=}{S}_2(\overline{\underset{=}{C}}_2)}{\partial \underset{=}{C}_2}, & s \ge s_b \end{cases} = \begin{cases} {}^{4}\underset{=}{\underset{=}{C}}_1, & 0 \le s \le s_a \\ {}^{4}\underset{=}{\underset{=}{C}}_1 + {}^{4}\underset{=}{\underset{=}{C}}_2, & s_a \le s \le s_b \\ {}^{4}\underset{=}{\underset{=}{C}}_2, & s \ge s_b \end{cases}, \tag{32}
$$

where

$$
{}^{4}\underset{=}{\underset{=}{C}}_1 = 2\frac{\partial \underset{=}{S}_1}{\partial \underset{=}{C}_1} = \underset{=}{\underset{=}{P}}_1 : \underset{=}{\underset{=}{\overline{C}}}_1 : {}^{4}\underset{=}{\underset{=}{P}}_1^{T} - \frac{2}{3}\left(\underset{=}{C}_1^{-1} \otimes \underset{=}{S}_1 + \underset{=}{S}_1 \otimes \underset{=}{C}_1^{-1}\right) + \frac{2}{3} J_1^{-2/3} \underset{=}{C}_1 : \overline{\underset{=}{S}}_1 \left(\underset{=}{C}_1^{-1} \oplus \underset{=}{C}_1^{-1} - \frac{1}{3}\underset{=}{C}_1^{-1} \otimes \underset{=}{C}_1^{-1}\right) \tag{33}
$$

and

$$
{}^{4}\underset{=}{\underset{=}{C}}_2 = 2\frac{\partial \underset{=}{S}_2}{\partial \underset{=}{C}_2} = \underset{=}{\underset{=}{P}}_2 : \underset{=}{\underset{=}{\overline{C}}}_2 : {}^{4}\underset{=}{\underset{=}{P}}_2^{T} - \frac{2}{3}\left(\underset{=}{C}_2^{-1} \otimes \underset{=}{S}_2 + \underset{=}{S}_2 \otimes \underset{=}{C}_2^{-1}\right) + \frac{2}{3} J_2^{-2/3} \underset{=}{C}_2 : \overline{\underset{=}{S}}_2 \left(\underset{=}{C}_2^{-1} \oplus \underset{=}{C}_2^{-1} - \frac{1}{3}\underset{=}{C}_2^{-1} \otimes \underset{=}{C}_2^{-1}\right) \tag{34}
$$

Here

$$
\underset{=}{\underset{=}{\overline{C}}}_1 = 2J_1^{-4/3} \frac{\partial \overline{\underset{=}{S}}_1}{\partial \overline{\underset{=}{C}}_1} = 2\alpha_1\gamma_1 e^{\gamma_1(\bar{I}_1 - 3)} \underset{=}{I} \otimes \underset{=}{I} \tag{35}
$$

and

$$
\underset{=}{\underset{=}{\overline{C}}}_2 = 2J_2^{-4/3} \frac{\partial \overline{\underset{=}{S}}_2}{\partial \overline{\underset{=}{C}}_2} = 2\alpha_2\gamma_2 e^{\gamma_2(\bar{I}_2 - 3)} \underset{=}{I} \otimes \underset{=}{I}. \tag{36}
$$

For derivation of (33) – (34) please refer to Appendix A.

3.0 VALIDATION OF THE FINITE ELEMENT CODE

The continuum mechanics model outlined in Chapter 2 was implemented in the general purpose finite element code ANSYS (version 10.0) [32] via the USERMAT subroutine (Appendix B). The developed code uses the pre- and post- processing capabilities as well as the nonlinear solvers of ANSYS. In order to test the validity of the code, several *test cases* have been created. Here, by a test case we mean a short input deck written in ANSYS Parametric Design Language (APDL), which is the input language of ANSYS. Each test case is expected to verify a certain aspect of the developed code.

3.1 DEGENERATE CASES

Note that in *degenerate cases* our model has to behave similarly to a standard hyperelastic material. Indeed, if we set

$$s_a = s_b = \infty, \tag{37}$$

$$s_a = s_b = 0 \tag{38}$$

or

$$s_a = 0,\ s_b = \infty \tag{39}$$

in eqn. (17), the expression for the strain energy density function becomes

$$\Psi = \Psi_{vol} + \Psi_1, \tag{40}$$

$$\Psi = \Psi_{vol} + \Psi_2 \tag{41}$$

or

$$\Psi = \Psi_{vol} + (\Psi_1 + \Psi_2) \tag{42}$$

respectively.

Clearly, in such cases the results generated by the proposed material model have to be identical to the results generated by simpler hyperelastic models. Thus we chose to compare our model with the ANSYS built-in Yeoh material model. The expression for the Yeoh strain energy density function follows:

$$\Psi = \sum_{i=1}^{N} c_i (\bar{I}_1 - 3)^i + \sum_{k=1}^{N} \frac{1}{d_k} (J-1)^{2k}. \tag{43}$$

For explanation of (43), please see Appendix B.

By approximating the exponential functions in (20) and (21) by their Taylor series, we generated a set of material parameters for the corresponding Yeoh material model

$$c_i = \frac{\alpha_1 \gamma^{i-1}}{2i!}, \tag{44}$$

$$c_i = \frac{\alpha_2 \gamma^{i-1}}{2i!} \tag{45}$$

and

$$c_i = \frac{(\alpha_1 + \alpha_2)\gamma^{i-1}}{2i!}, \tag{46}$$

where *i=1..10* for the cases (37), (38) and (39) respectively.

For each of the three degenerate cases (37), (38) and (39) six test cases have been created (a total of eighteen tests). Five of the tests were one-element uniaxial, biaxial, equitriaxial, non-equitriaxial tension and simple shear tests, and one test examined a more complex geometry.

Material constants chosen for the simple one-element tests were borrowed from [25], and are summarized in Table 1.

Table 1. Material parameters

Parameters		α_1	α_2	γ_1	γ_2	d
Values	Degenerate case $s_a=0,\ s_b=\infty$	*3550 Pa*	*3550 Pa*	*0.62*	*0.62*	$10^{-6}\ Pa^{-1}$
	Other degenerate cases	*7100 Pa*	*7100 Pa*	*0.62*	*0.62*	$10^{-6}\ Pa^{-1}$

3.1.1 One-Element Tests

The geometry for the one-element tests is a cube of unit dimension, consisting of a single 3D 8-node finite element, with displacement boundary conditions applied. The boundary conditions for these tests are illustrated in Figure 6 – 9 and summarized in Table 2.

Table 2. One-Element Tests and Boundary Conditions

Test type	Uniaxial tension	Biaxial tension	Equitriaxial tension	Nonequitriaxial tension	Simple Shear
Boundary conditions	$u_x=1.0$	$u_x=0.7$ $u_z=0.7$	$u_x=0.5$ $u_y=0.5$ $u_z=0.5$	$u_x=0.5$ $u_y=1.0$ $u_z=0.8$	$u_x=0.5$

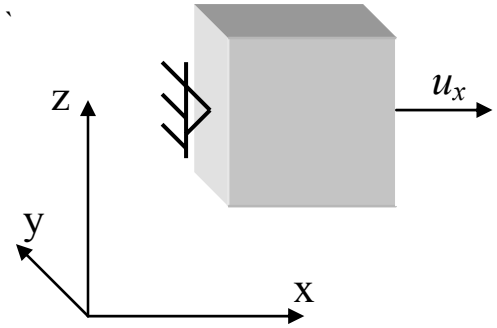

Figure 6. Uniaxial tension test

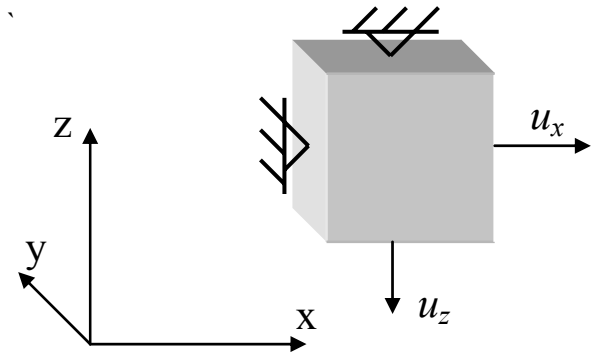

Figure 7. Biaxial tension test

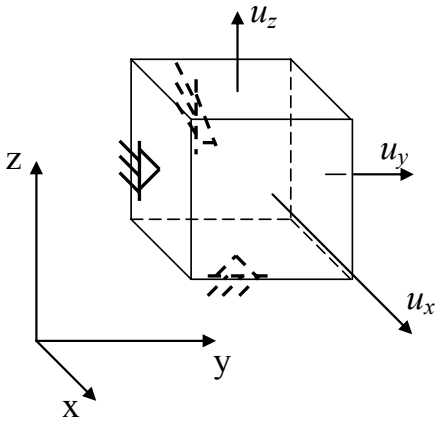

Figure 8. Triaxial tension test

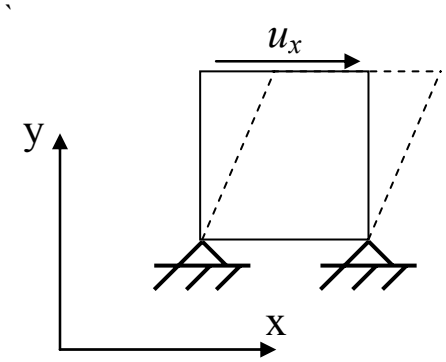

Figure 9. Simple shear test

The resultant *x*-components of the Cauchy stress tensor for each of the tests are provided in Table 3. As can be seen from Table 3, one-element tests of the multi-mechanism material model exactly matched stress-strain results with the Yeoh material model (error $\varepsilon = 0.0\%$).

Table 3. Results of the One-Element Tests: x-component of Cauchy stress tensor

Degenerate case	Test type	**Multi-Mechanism Model**	**Yeoh Model**	**Error, %**
$s_a=s_b=\infty$	Uniaxial tension	*82159.8*	*82159.4*	$4.9 \cdot 10^{-4}$
	Biaxial tension	*103595*	*103588*	$6.8 \cdot 10^{-3}$
	Equitriaxial tension	$0.475 \cdot 10^{7}$	$0.475 \cdot 10^{7}$	*0*
	Nonequitriaxial tension	$0.879959 \cdot 10^{7}$	$0.879959 \cdot 10^{7}$	*0*
	Simple Shear	*2068*	*2068*	*0*
$s_a=0,\ s_b=\infty$	Uniaxial tension	*82159.8*	*82159.4*	$4.9 \cdot 10^{-4}$
	Biaxial tension	*103595*	*103588*	$6.8 \cdot 10^{-3}$
	Equitriaxial tension	$0.475 \cdot 10^{7}$	$0.475 \cdot 10^{7}$	*0*
	Nonequitriaxial tension	$0.879959 \cdot 10^{7}$	$0.879959 \cdot 10^{7}$	*0*
	Simple Shear	*2068*	*2068*	*0*
$s_a=s_b=0$	Uniaxial tension	*82159.8*	*82159.4*	$4.9 \cdot 10^{-4}$
	Biaxial tension	*103595*	*103588*	$6.8 \cdot 10^{-3}$
	Equitriaxial tension	$0.475 \cdot 10^{7}$	$0.475 \cdot 10^{7}$	*0*
	Nonequitriaxial tension	$0.879959 \cdot 10^{7}$	$0.879959 \cdot 10^{7}$	*0*
	Simple Shear	*2068*	*2068*	*0*

3.1.2 Cantilevered Plate

Consider a cantilevered plate with vertical deflection applied at its free end (Figure 10).

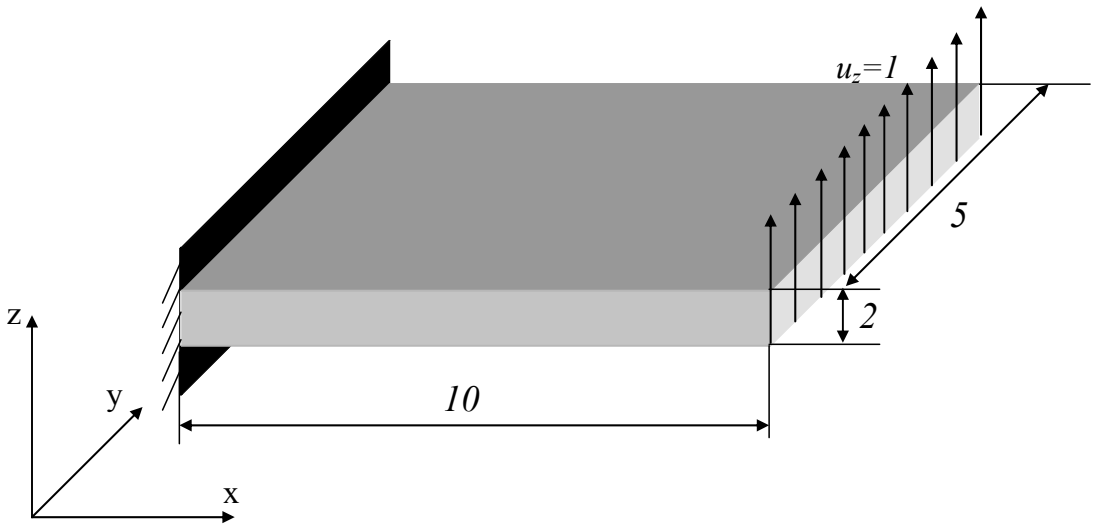

Figure 10. Cantilevered plate

Two finite element models have been created, one utilizing the multi-mechanism material model, another one utilizing the Yeoh material model, the parameters for which have been chosen according to Table 1 and equations (44) – (46). Each finite element model consists of 100 3D 8-node elements. Von Mises stress results, obtained utilizing the models, are plotted in Figure 11. As shown, the stress field generated by the multi-mechanism material model (left) is indistinguishable from the one generated by the Yeoh material model (right).

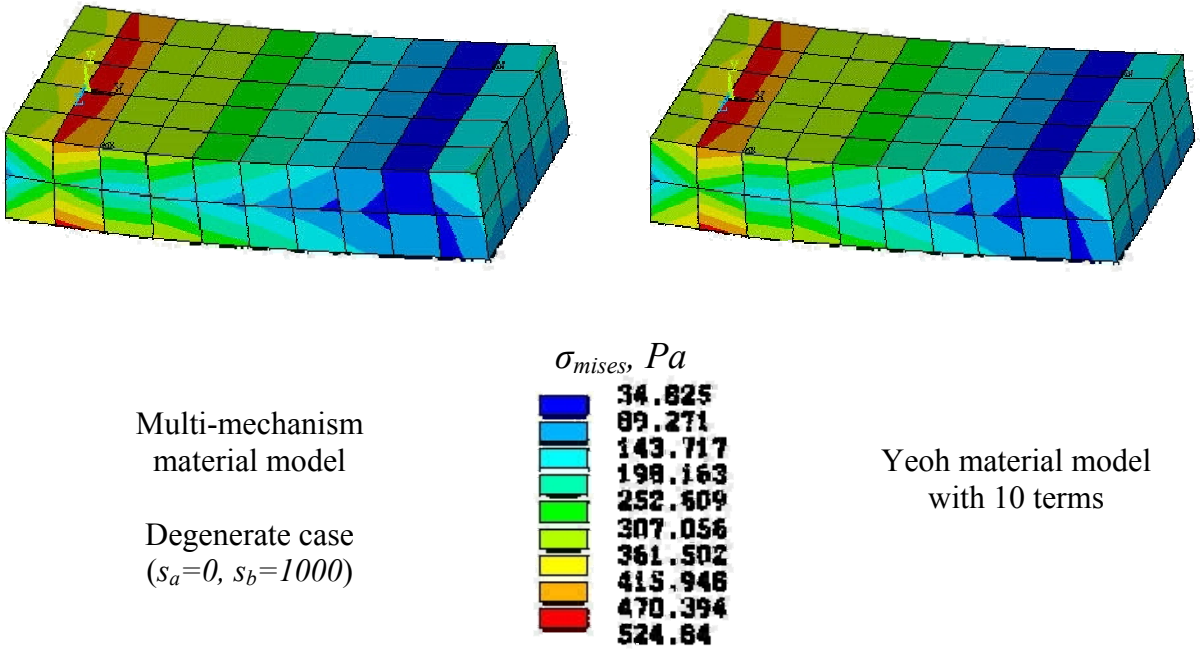

Figure 11. Bending of a cantilevered plate

3.2 ANALYTICAL SOLUTION

For some simple geometric configurations it is possible to find analytical solutions to the constitutive equations outlined in Section 3. This provides another means of verifying the finite element code. In this section we will look at the uniaxial extension of a cube and pressure inflation of a cylinder to verify the proposed model.

3.2.1 Uniaxial tension

Consider uniaxial tension of a multi-mechanism cube of a unit dimension (Figure 6). The deformation gradient in this case takes a relatively simple form:

$$F_1 = \begin{bmatrix} \lambda_1 & 0 & 0 \\ 0 & \lambda_2 & 0 \\ 0 & 0 & \lambda_2 \end{bmatrix}. \tag{47}$$

From (16) the deformation parameter s becomes:

$$s = \lambda_1 \lambda_2^2 - 3\,. \tag{48}$$

Similarly the deformation gradient $\underline{\underline{F}}_2$ relative to the reference configuration κ_2, right Cauchy-Green tensors $\underline{\underline{C}}_1$ and $\underline{\underline{C}}_2$, Jacobians J_1 and J_2, modified deformation gradients $\overline{\underline{\underline{F}}}_1$ and $\overline{\underline{\underline{F}}}_2$, and modified right Cauchy-Green Tensors $\overline{\underline{\underline{C}}}_1$ and $\overline{\underline{\underline{C}}}_2$ can be expressed in terms of principal stretches λ_1 and λ_2 via equations (9) – (10) and (11) – (12). Second Piola-Kirchhoff stress $\underline{\underline{S}}$ can be determined from equations (22) – (29). Finally, applying

$$\underline{\underline{\sigma}} = \underline{\underline{\sigma}}_{vol} + \underline{\underline{\sigma}}_{iso} \tag{49}$$

where

$$\underline{\underline{\sigma}}_{vol} = 2J_1^{-1}\underline{\underline{F}}_1 \cdot \frac{\partial \Psi_{vol}}{\partial \underline{\underline{C}}} \cdot \underline{\underline{F}}_1^T = J_1^{-1} J_1 p \underline{\underline{I}} = p\underline{\underline{I}} \tag{50}$$

and

$$\underline{\underline{\sigma}}_{iso} = \begin{cases} J_1^{-1}\underline{\underline{F}}_1 \cdot \underline{\underline{S}}_1 \cdot \underline{\underline{F}}_1^T, & 0 \le s \le s_a \\ J_1^{-1}\underline{\underline{F}}_1 \cdot \underline{\underline{S}}_1 \cdot \underline{\underline{F}}_1^T + J_2^{-1}\underline{\underline{F}}_2 \cdot \underline{\underline{S}}_2 \cdot \underline{\underline{F}}_2^T, & s_a \le s \le s_b\,, \\ J_2^{-1}\underline{\underline{F}}_2 \cdot \underline{\underline{S}}_2 \cdot \underline{\underline{F}}_2^T, & s \ge s_b \end{cases} \tag{51}$$

we obtain the following expressions for the principal Cauchy stresses in terms of λ_1 and λ_2:

for $s < s_a$

$$\sigma_{11} = \frac{2}{d}(\lambda_1\lambda_2^2 - 1) + \frac{2}{3}\alpha_1 \exp(\gamma_1((\frac{\lambda_1}{\lambda_2})^{4/3} + 2(\frac{\lambda_1}{\lambda_2})^{-2/3} - 3)(\lambda_1\lambda_2^2)^{-5/3}(\lambda_1^2 - \lambda_2^2), \tag{52}$$

$$\sigma_{22} = \frac{2}{d}(\lambda_1\lambda_2^2 - 1) + \frac{1}{3}\alpha_1 \exp(\gamma_1((\frac{\lambda_1}{\lambda_2})^{4/3} + 2(\frac{\lambda_1}{\lambda_2})^{-2/3} - 3)(\lambda_1\lambda_2^2)^{-5/3}(\lambda_2^2 - \lambda_1^2), \tag{53}$$

for $s_a \leq s < s_b$

$$\sigma_{11} = \frac{2}{d}(\lambda_1\lambda_2^2 - 1) + \frac{2}{3}\alpha_1 \exp(\gamma_1((\frac{\lambda_1}{\lambda_2})^{4/3} + 2(\frac{\lambda_1}{\lambda_2})^{-2/3} - 3)(\lambda_1\lambda_2^2)^{-5/3}(\lambda_1^2 - \lambda_2^2)$$

$$+ \frac{2}{3}\alpha_2 \exp(\gamma_2((\frac{\lambda_1\lambda_2^a}{\lambda_1^a\lambda_2})^{4/3} + 2(\frac{\lambda_1\lambda_2^a}{\lambda_1^a\lambda_2})^{-2/3} - 3)(\frac{\lambda_1}{\lambda_1^a}(\frac{\lambda_2}{\lambda_2^a})^2)^{-5/3}((\frac{\lambda_1}{\lambda_1^a})^2 - (\frac{\lambda_2}{\lambda_2^a})^2), \tag{54}$$

$$\sigma_{22} = \frac{2}{d}(\lambda_1\lambda_2^2 - 1) + \frac{1}{3}\alpha_1 \exp(\gamma_1((\frac{\lambda_1}{\lambda_2})^{4/3} + 2(\frac{\lambda_1}{\lambda_2})^{-2/3} - 3)(\lambda_1\lambda_2^2)^{-5/3}(\lambda_2^2 - \lambda_1^2)$$

$$+ \frac{1}{3}\alpha_2 \exp(\gamma_2((\frac{\lambda_1\lambda_2^a}{\lambda_1^a\lambda_2})^{4/3} + 2(\frac{\lambda_1\lambda_2^a}{\lambda_1^a\lambda_2})^{-2/3} - 3)(\frac{\lambda_1}{\lambda_1^a}(\frac{\lambda_2}{\lambda_2^a})^2)^{-5/3}((\frac{\lambda_2}{\lambda_2^a})^2 - (\frac{\lambda_1}{\lambda_1^a})^2), \tag{55}$$

and for $s \geq s_b$

$$\sigma_{11} = \frac{2}{d}(\lambda_1\lambda_2^2 - 1) + \frac{2}{3}\alpha_2 \exp(\gamma_2((\frac{\lambda_1\lambda_2^a}{\lambda_1^a\lambda_2})^{4/3} + 2(\frac{\lambda_1\lambda_2^a}{\lambda_1^a\lambda_2})^{-2/3} - 3)(\frac{\lambda_1}{\lambda_1^a}(\frac{\lambda_2}{\lambda_2^a})^2)^{-5/3}((\frac{\lambda_1}{\lambda_1^a})^2 - (\frac{\lambda_2}{\lambda_2^a})^2), \tag{56}$$

$$\sigma_{22} = \frac{2}{d}(\lambda_1\lambda_2^2 - 1) + \frac{1}{3}\alpha_2 \exp(\gamma_2((\frac{\lambda_1\lambda_2^a}{\lambda_1^a\lambda_2})^{4/3} + 2(\frac{\lambda_1\lambda_2^a}{\lambda_1^a\lambda_2})^{-2/3} - 3)(\frac{\lambda_1}{\lambda_1^a}(\frac{\lambda_2}{\lambda_2^a})^2)^{-5/3}((\frac{\lambda_2}{\lambda_2^a})^2 - (\frac{\lambda_1}{\lambda_1^a})^2), \tag{57}$$

where λ_1^a and λ_2^a are values of principal stretches corresponding to $s = s_a$.

These equations can be solved numerically to obtain a dependency of the first principle stress on the first principle stretch.

In order to verify the multi-mechanism material model, a finite element model, consisting of a single 3D 8-node finite element was created.

Material constants chosen for the analysis, borrowed from [25], are summarized in Table 4.

Table 4. Material parameters for the uniaxial tension test

Parameters	α_1	α_2	γ_1	γ_2	s_a	s_b	d
Values	*7100 Pa*	*31000 Pa*	*0.62*	*1.87*	*1.4*	*3.48*	$10^{-6}\ Pa^{-1}$

Figure 12 shows stress-stretch curves obtained analytically and by means of the finite element analysis. As we can see the results match well.

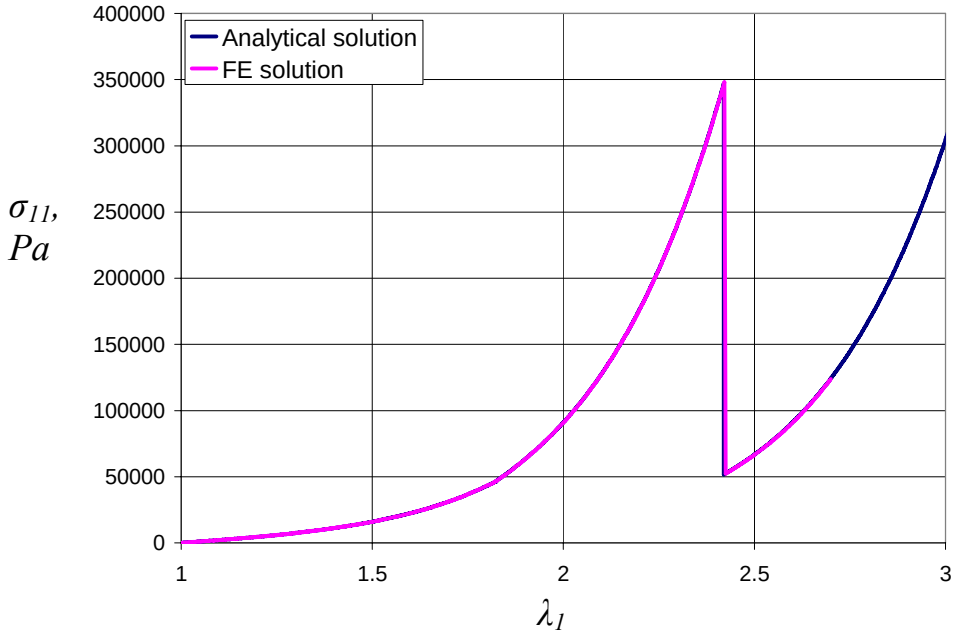

Figure 12. First principle stress vs. first principle stretch. Analytical and finite element solutions

3.2.2 Pressure inflation of a cylinder

Consider a hollow thick-walled cylinder that incorporates a multi-mechanism material and has an internal radius R_i and an external radius R_o. The cylinder is subjected to internal pressure P and constrained in z-direction at both ends (Figure 14).

A finite element model, consisting of 20 2D-axisymmetric 4-node finite elements was created (Figure 13). Axisymmetry boundary conditions have been utilized in order to reduce the solution time and minimize computational costs. Material properties (taken from [25]), the model geometry, and the finite element properties are summarized in Table 5.

Table 5. Geometry of the cylinder and material parameters

Parameter	Value	Units
α_1	7100	*Pa*
α_2	31000	*Pa*
γ_1	0.62	–
γ_2	1.87	–
s_a	1.4	–
s_b	3.48	–
Wall thickness	$1.0 \cdot 10^{-4}$	*m*
Inner radius	$0.28 \cdot 10^{-4}$	*m*
Height of the cylinder	$3.33 \cdot 10^{-6}$	*m*

In order to obtain the analytical solution of this problem, we assume that the material is incompressible. The deformation gradient for the material volume located at the outer surface of the cylinder becomes:

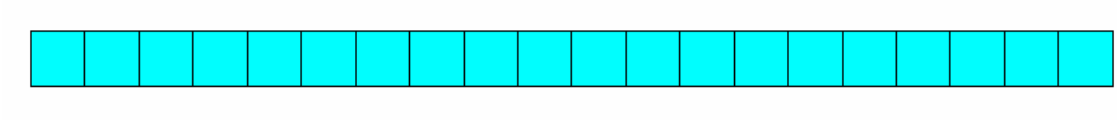

(a)

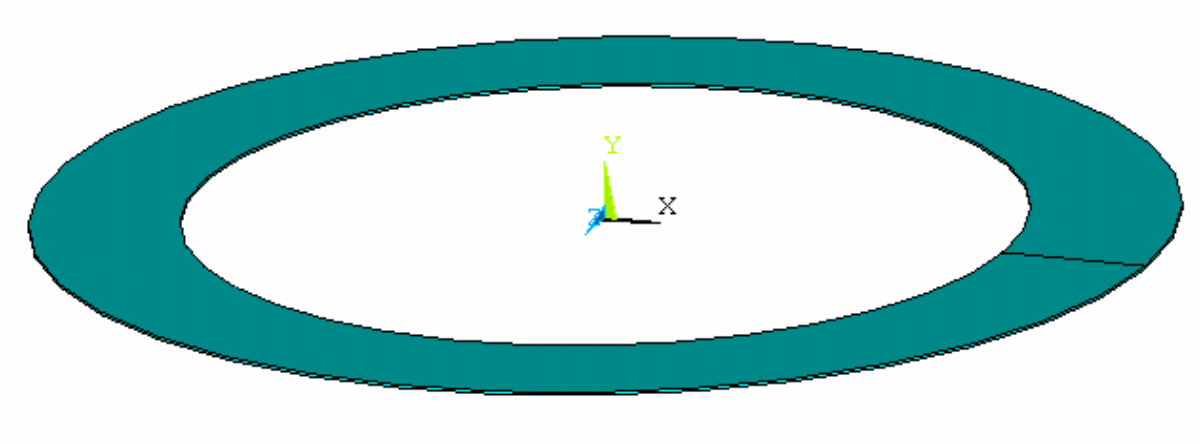

(b)

Figure 13. 2d axisymmetric finite element model (a) and expanded shape (b) of the cylinder

$$F_1 = \begin{bmatrix} \lambda_\theta & 0 & 0 \\ 0 & \lambda_r & 0 \\ 0 & 0 & 1/(\lambda_\theta \lambda_r) \end{bmatrix} \tag{37}$$

If the radial displacement at the outer surface is denoted as Δr, the principle stretches can be expressed as

$$\lambda_\theta = 1 + \frac{\Delta r}{R_o}, \text{ and } \lambda_r = \frac{R_o}{R_o + \Delta r}. \tag{38) – (39}$$

From (16) the deformation parameter s becomes:

$$s = \frac{R_o^2}{(R_o + \Delta r)^2} + (1 + \frac{\Delta r}{R_0})^2 - 2 \tag{40}$$

Utilizing results from Section 2.2, taking into consideration the boundary condition

$$\sigma_{rr}\Big|_{r=R_o} = 0 \tag{41}$$

and assuming that the deformation parameter s reaches its critical values s_a or s_b simultaneously throughout the wall of the cylinder, the expression for the circumferential Cauchy stress can be obtained.

For $s < s_a$ we have

$$\sigma_{\theta\theta} = \alpha_1 \exp[\gamma_1(\lambda_r^2 + \lambda_\theta^2 - 2)]\left(\lambda_\theta^2 - \lambda_r^2\right) \tag{42}$$

Denoting the values that principal stretches take when $s = s_a$ as λ_θ^a and λ_r^a and defining

$$\lambda_\theta^{(2)} = \frac{\lambda_\theta}{\lambda_\theta^a} \tag{43}$$

and

$$\lambda_r^{(2)} = \frac{\lambda_r}{\lambda_r^a} \tag{44}$$

we have for $s_a \leq s < s_b$

$$\sigma_{\theta\theta} = \alpha_1 \exp[\gamma_1(\lambda_r^2 + \lambda_\theta^2 - 2)]\left(\lambda_\theta^2 - \lambda_r^2\right) + \alpha_2 \exp[\gamma_2((\lambda_r^{(2)})^2 + (\lambda_\theta^{(2)})^2 - 2)][(\lambda_\theta^{(2)})^2 - (\lambda_r^{(2)})^2] \tag{45}$$

and for $s \geq s_b$

$$\sigma_{\theta\theta} = \alpha_2 \exp[\gamma_2((\lambda_r^{(2)})^2 + (\lambda_\theta^{(2)})^2 - 2)][(\lambda_\theta^{(2)})^2 - (\lambda_r^{(2)})^2] \,. \tag{46}$$

In equations (42), (45) and (46) we obtain the circumferential stress at the outer surface of the cylinder as a function of the radial displacement at the outer surface.

Figure 15 shows the stress-displacement curves obtained analytically and by means of the finite element analysis. As illustrated in the figure, the analytical solution provides a very close match to the finite element solution of the problem. This example is particularly important, because it represents the physical geometry of an idealized blood vessel (cylinder).

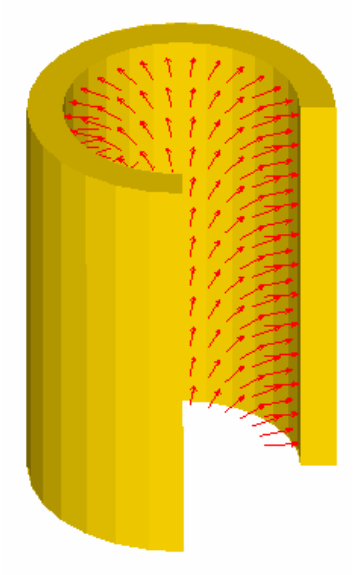

Figure 14. Hollow thick-walled cylinder subjected to internal pressure

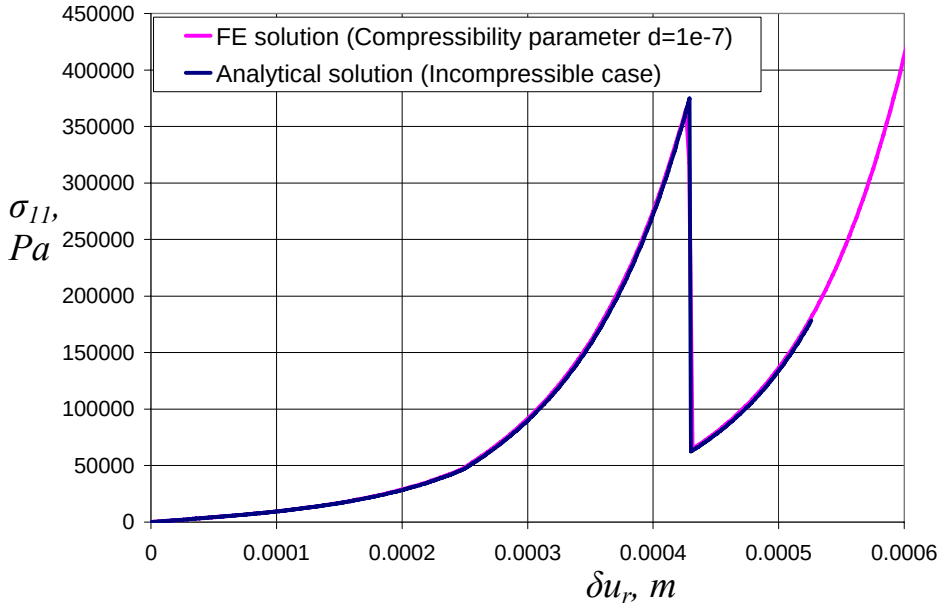

Figure 15. Comparison of the analytical and finite element solutions of the cylindrical expansion problem. First principal stress σ_{11} at the outer edge vs. inner radius increment δu_r

3.2.3 Reproducing experimental results by Scott et al. [9]

Let us now attempt to numerically reproduce experimental results of [9] (Figure 3). We consider a hollow multi-mechanism cylinder (representing a blood vessel) with pressure applied from within. We assume that the ends of the cylinder are constrained from moving in the axial direction. A finite element model corresponding to this problem is similar to the one shown in Figure 13, only it consists of 30 2D axisymmetric 4-node finite elements, rather than 20. The geometry of the cylinder and material properties [25] are summarized in Table 6.

Table 6. Geometry of the vessel and material parameters

Parameter	Value	Units
α_1	8900	*Pa*
α_2	39000	*Pa*
γ_1	0.62	–
γ_2	1.87	–
s_a	1.4	–
s_b	3.48	–
Wall thickness	$1.0 \cdot 10^{-4}$	*m*
Inner radius	$0.28 \cdot 10^{-3}$	*m*
Blood vessel length considered	$0.2 \cdot 10^{-5}$	*m*

We conduct several numerical experiments varying the value of the compressibility parameter *d*. When *d* is small enough, the material response stops being dependent on *d*, and the material can be considered nearly incompressible. The results, obtained for the nearly incompressible material, can be compared with [25].

Tension vs. radius graphs obtained numerically, superimposed on experimental data from [9], are shown in Figure 16.

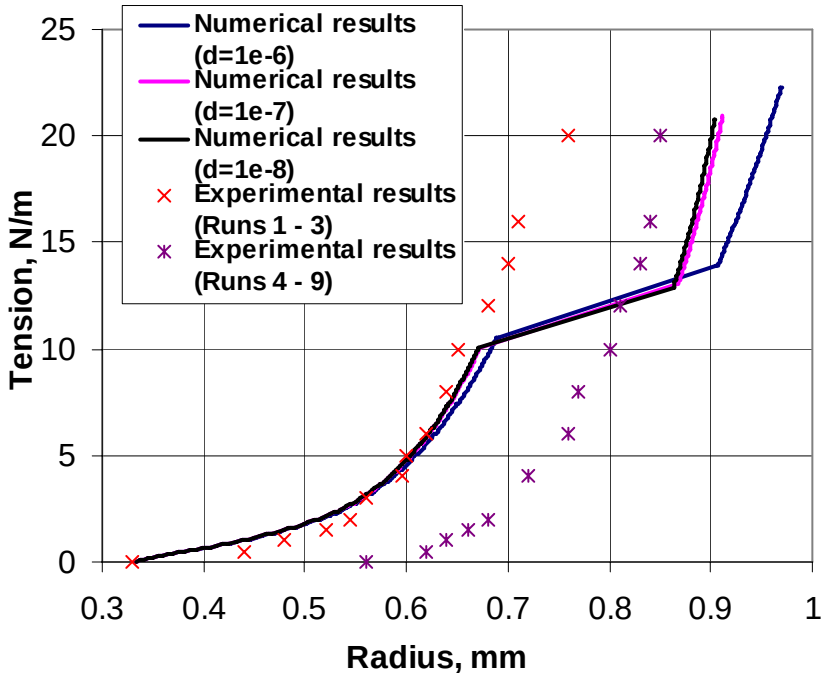

Figure 16. Tension vs. radius results obtained numerically and experimental data from Scott et al. [9]

As we can see, the mechanical response of the multi-mechanism model follows the first set of experimental data (Runs 1 – 3), and then, after (presumably) the rupture of elastin fibers, slides to the second set of points (Runs 4 – 9). From Figure 16 we may conclude that

(a) Our numerical model is shown to qualitatively repeat experimental results by Scott et al., and

(b) The value of $d=1\cdot10^{-7}\ Pa^{-1}$ is sufficiently small for our material to be considered nearly incompressible.

The difference between the numerical results and the experimental data can possibly be attributed to the fact that material parameters (Table 6) that we used in the simulation were obtained by Wulandana and Robertson [25] who performed curve fitting for the case of pressure inflation of a cylinder in membrane formulation, whereas we consider a 3D case, taking the thickness of the cylinder into account.

4.0 SIMULATION OF BALLOON ANGIOPLASTY

Angioplasty (from Greek *angio* vessel and *plassein* to form) is a medical procedure used to mechanically widen a narrowed (*stenosis*) or obstructed blood vessel, and restore blood flow. The obstruction is typically a result of atherosclerosis.

During balloon angioplasty a catheter with a cylindrical balloon surrounding it is inserted into the blood vessel. Once in position, the balloon is inflated with pressure between *9* and *15* atmospheres [33] in order to force the narrowed vessel to expand.

Angioplasty is commonly referred to as a *percutaneous* (minimally invasive) method, and is often preferred to surgery. It is usually performed on coronary arteries (*percutaneous transluminal coronary angioplasty* – PTCA), leg arteries, especially the common iliac, external iliac, superficial femoral and popliteal arteries, and renal arteries [33]. Recently, angioplasty has been used to treat *carotid stenosis* in carotid arteries [34].

Our goal here is to illustrate how the multi-mechanism material model can be used to model the process of angioplasty. Due to the lack of experimental data we do not presume to verify what actually happens during angioplasty, but merely try to understand how a foreign object, when inserted into a cylindrical vessel, affects its biomechanics.

Again we consider a multi-mechanism hollow cylinder, its ends constrained in the axial direction, pressure applied from within. A 2D finite element model consisting of 1560 2D 4-node axisymmetric finite elements is shown in Figure 17. The balloon is modeled as a 2D rigid target.

Since the only source of material data pertaining to the multi-mechanism model is [25], we hereby adopt material parameters and vessel geometry, pertaining to the anterior cerebral artery, from this paper. Material properties used in the analysis, as well as the geometry of the problem are summarized in Table 7.

The finite element problem is solved in two steps. First, a uniform pressure of *10,000 Pa* is applied to the inner surface of the cylinder. The resultant shape is shown in Figure 18. As we can see from Figure 18, a part of the cylinder is in the first (elastin only) deformation mechanism, and another part is in the second (both mechanisms active) deformation mechanism. Next the rigid target starts to move toward the inner surface of the cylinder, until it comes into contact with it, and starts to mechanically interact with the vessel wall (Figure 19).

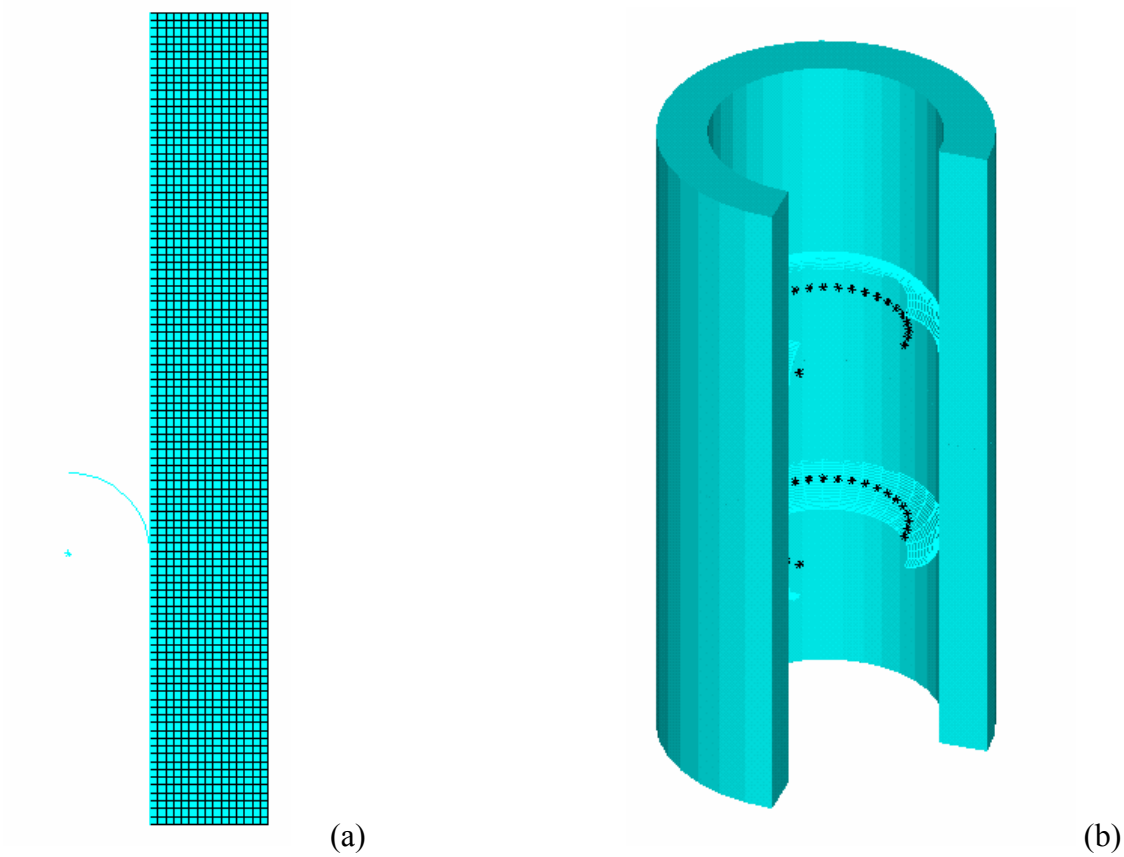

Figure 17. 2d axisymmetric finite element model (a) and expanded shape (b) of the artery

Table 7. Material parameters and model geometry

Parameter	Value	Units
α_1	7100	*Pa*
α_2	31000	*Pa*
γ_1	0.62	–
γ_2	1.87	–
s_a	1.4	–
s_b	3.48	–
Wall thickness	$1.0 \cdot 10^{-4}$	*m*
Inner radius	$0.23 \cdot 10^{-3}$	*m*
Blood vessel length considered	$2 \cdot 0.69 \cdot 10^{-3}$	*m*
Initial radius of the balloon	$0.23 \cdot 10^{-3}$	*m*

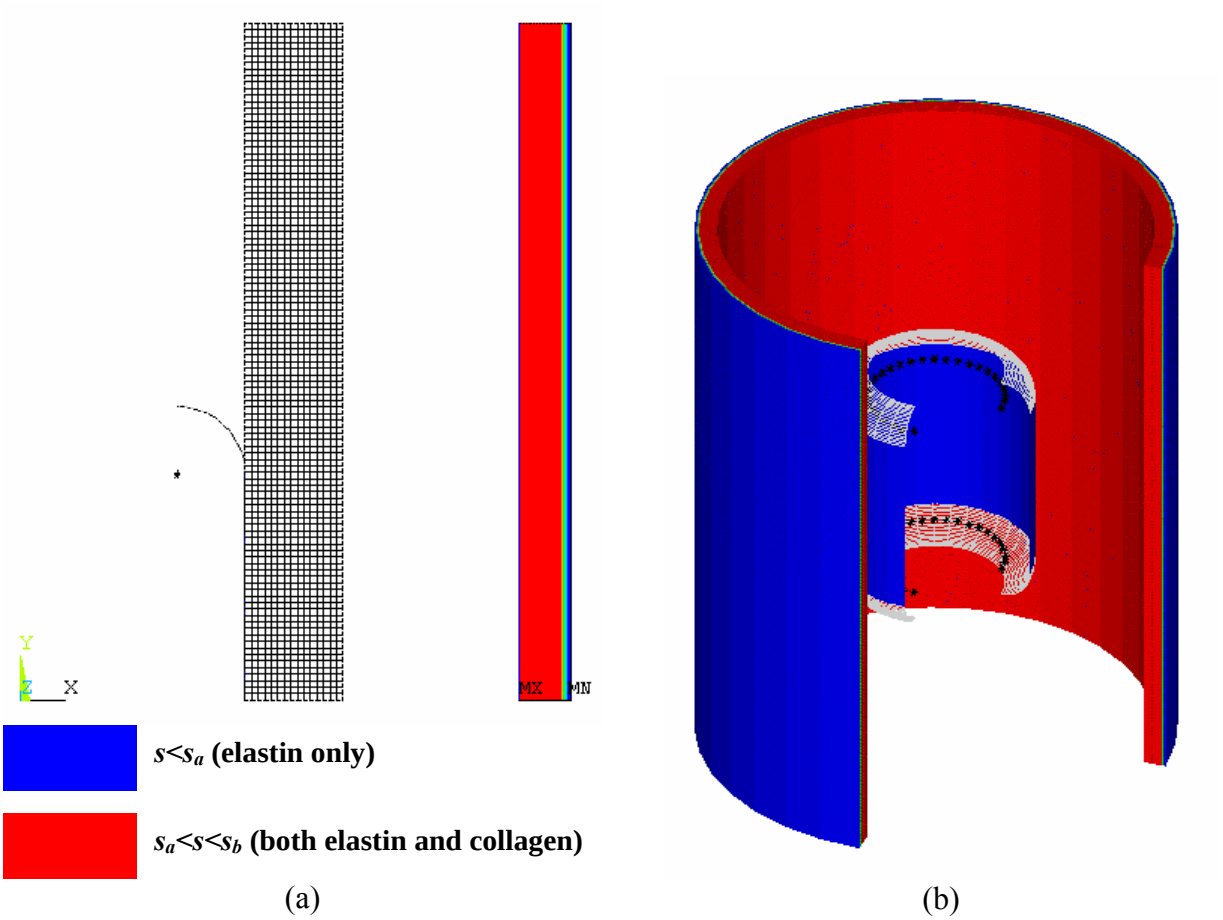

Figure 18. Deformed shape of the vessel corresponding to applied internal pressure: (a) 2D axisymmetric, (b) 3D expanded

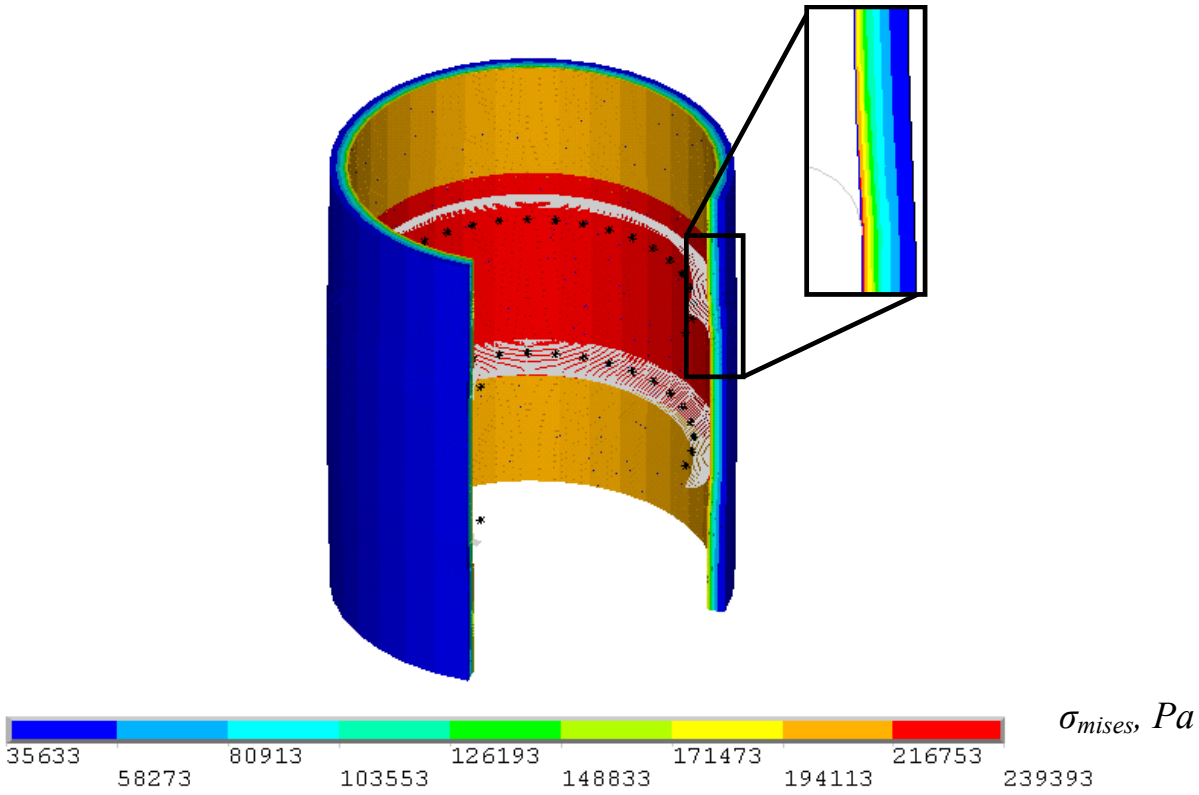

Figure 19. Von Mises stress distribution at the moment of contact of the balloon with the artery wall

Figure 19 shows the stress distribution at the moment of contact. As can be expected, maximum stresses arise in the area of contact.

As the rigid target continues its motion, the onset of elastin rupture can be observed (Figure 20). As can be seen in Figure 20, the areas of the vessel near the area of contact are in the state of the third deformation mechanism, whereby elastin has ruptured. This should be avoided during the actual angioplasty.

Figure 21 shows a resultant distribution of equivalent stresses. An interesting phenomenon can be observed: the maximum stresses do not arise near the zone of contact, but rather are located inside the vessel's wall. This is explained by the fact that the areas near the

zone of contact are in the third deformation mechanism (when elastin is ruptured), and thus, are at a lower stress level.

Perhaps the most important work concerning finite element analysis of angioplasty has been performed by Holzapfel et al [35, 36]. The researchers modeled the artery tissue as a multi-layered anisotropic hyperelastic material. Current work does not take anisotropy into account, although it is capable of describing collagen recruitment and elastin rupture. Further research must be carried out in order to determine the relative importance of the phenomena mentioned above.

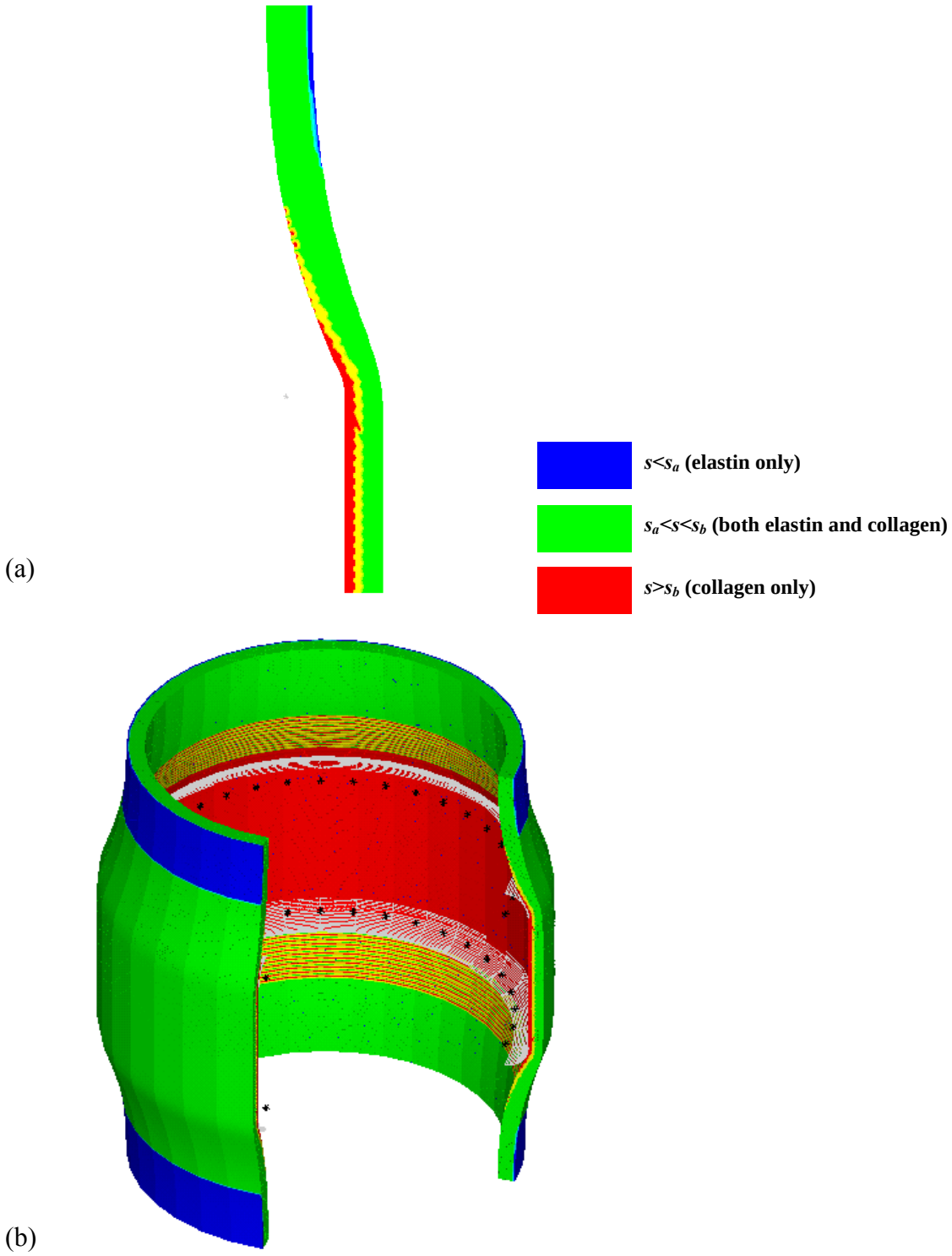

Figure 20. Deformed shape of the vessel corresponding to applied internal pressure and contact of the deployed balloon with the internal surface: (a) 2D axisymmetric, (b) 3D expanded

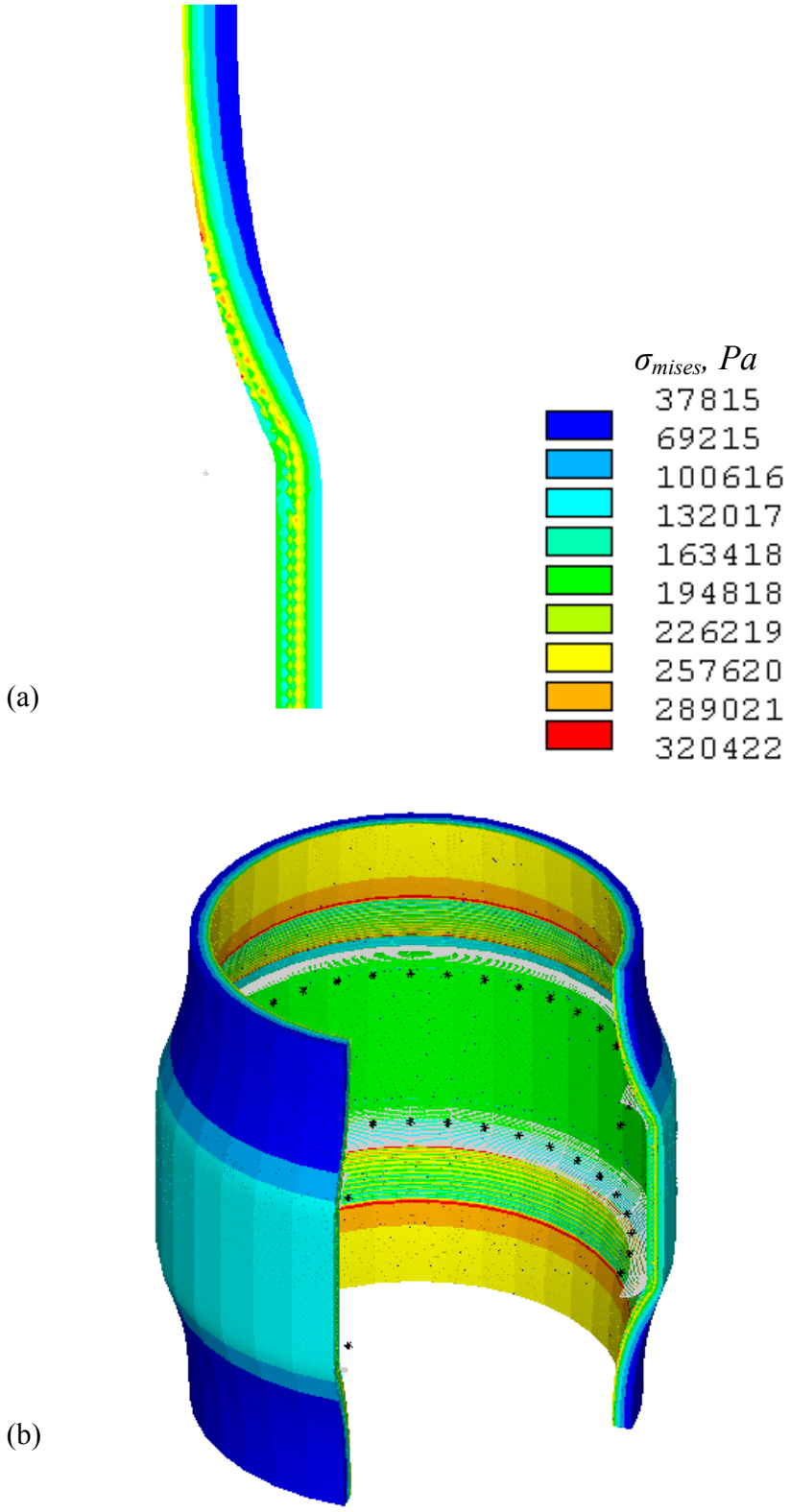

Figure 21. Deformed shape of the vessel corresponding to applied internal pressure and contact of the deployed balloon with the internal surface: (a) 2D axisymmetric, (b) 3D expanded. Equivalent stress distribution

5.0 SIMULATION OF A FUSIFORM ANEURYSM FORMATION

In order to simulate aneurysm formation and growth a finite element model (shown in Figure 22) was created. The properties of the finite element model are summarized in Table 8. The model geometry, as well as material properties (Table 9. Material parameters), were adopted from [25]. It is an axisymmetric model, and therefore only a cross-section has been considered. An expanded view of the model is shown in Figure 23. It is well known (c.f. [7], [37 – 39]) that aneurysms develop from an imperfection in the arterial wall ("bleb"). Thus a small geometrical imperfection has been introduced into the finite element model (Figure 22). A pressure load of *30,000 Pa* is applied to the inner surface of the cylinder. At the top end of the cylinder symmetry boundary conditions have been applied.

A question of properly applying boundary conditions at the bottom end of the cylinder is not trivial. Clearly, simply constraining it from moving in the axial direction will not be accurate since axial stresses are obviously present inside the blood vessel's wall. Another simplification would be to seal one end of the cylinder, and apply the same pressure of *30,000 Pa* to the seal (Figure 24). Apparently, the truth lies somewhere in the middle. In the current work we have adopted the latter approach, even though it is a simplification. At the bottom end of the cylinder an axisymmetric Shell208 element (with very low stiffness properties assigned to it) has been created, connecting the origin with the inner surface of the cylinder. The pressure load of

30,000 Pa has been applied to this element, and the vertical displacement degrees of freedom of all nodes at the bottom end of the cylinder have been coupled.

Table 8. Geometrical and finite element properties of the finite element model

Geometrical properties	**Finite element properties**
• Wall thickness: $0.125 \cdot 10^{-3}$ m • Inner radius: $0.2675 \cdot 10^{-03}$ m • Blood vessel length considered: $3.21 \cdot 10^{-03}$ m • Thickness at the imperfection: $0.0875 \cdot 10^{-03}$ m	• Element type: Plane182 axisymmetric • Number of elements: 2401 • Number of nodes: 2577

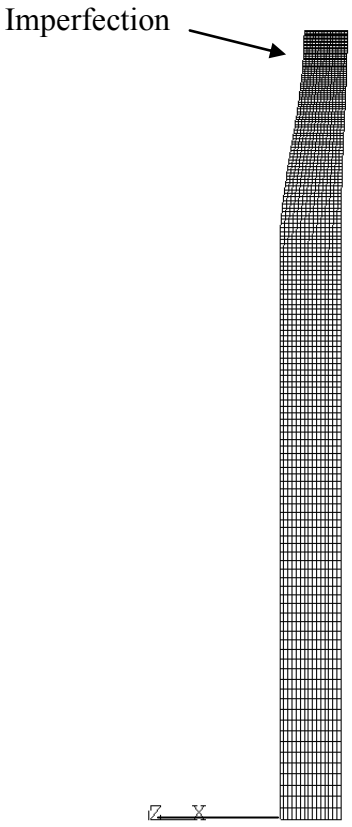

Figure 22. Finite element model

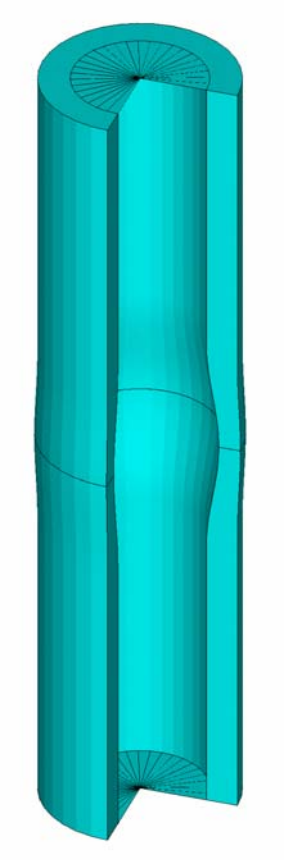

Figure 23. Expanded view of the model

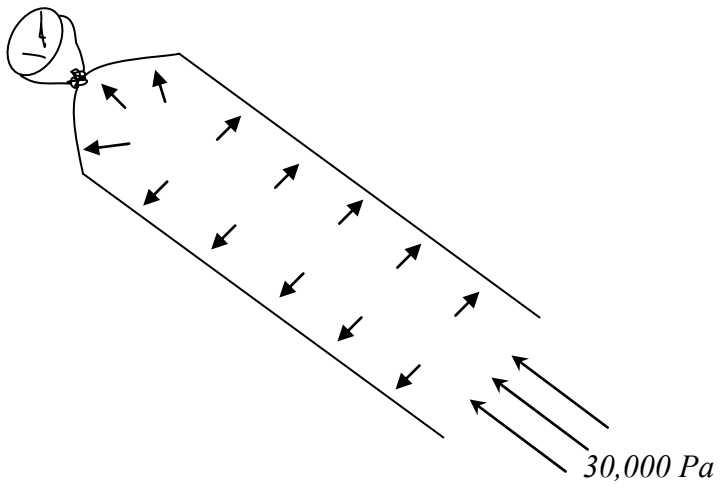

Figure 24. A simplified way of applying boundary conditions

As we begin to pressurize the cylinder, elastin is the only load bearing component (first deformation mechanism active, $s < s_a$). As we continue the loading, the second deformation mechanism turns on (collagen recruitment, $s_a < s < s_b$) (Figure 25). Figure 26 shows Von Mises stress distribution, corresponding to the moment of collagen recruitment. As can be expected, maximum stresses arise in the area of the geometrical imperfection. As the applied pressure is further increased, the onset of elastin rupture can be observed (Figure 27). As can be seen, the stresses are no longer monotonously decreasing from the inner toward the outer side of the cylinder wall. Rather, they appear to reach a local minimum around the middle of the wall. This is explained by the fact that with rupture of elastin, the multi-mechanism material becomes more compliant.

The resultant deformed shape of the model is shown in Figure 28. The elements, for which $s_a<s<s_b$ are plotted in green, whereas those for which $s>s_b$ are plotted in red. The expanded deformed shape is shown in Figure 28 (b). For comparison, Figure 29 shows a schematic of a fusiform aneurysm [40].

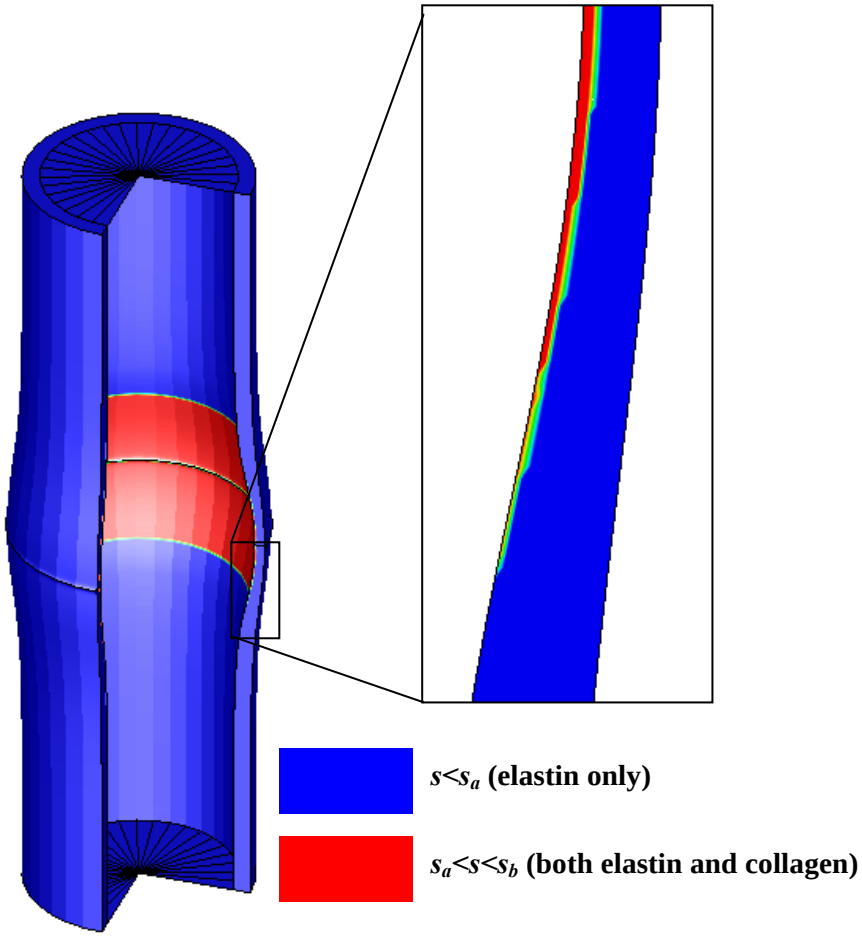

Figure 25. Collagen recruitment

Table 9. Material parameters

Parameter	Value	Dimension
α_1	7100	Pa
α_2	31000	Pa
γ_1	0.62	–
γ_2	1.87	–
s_a	1.4	–
s_b	3.48	–
d	10^{-5}	Pa^{-1}

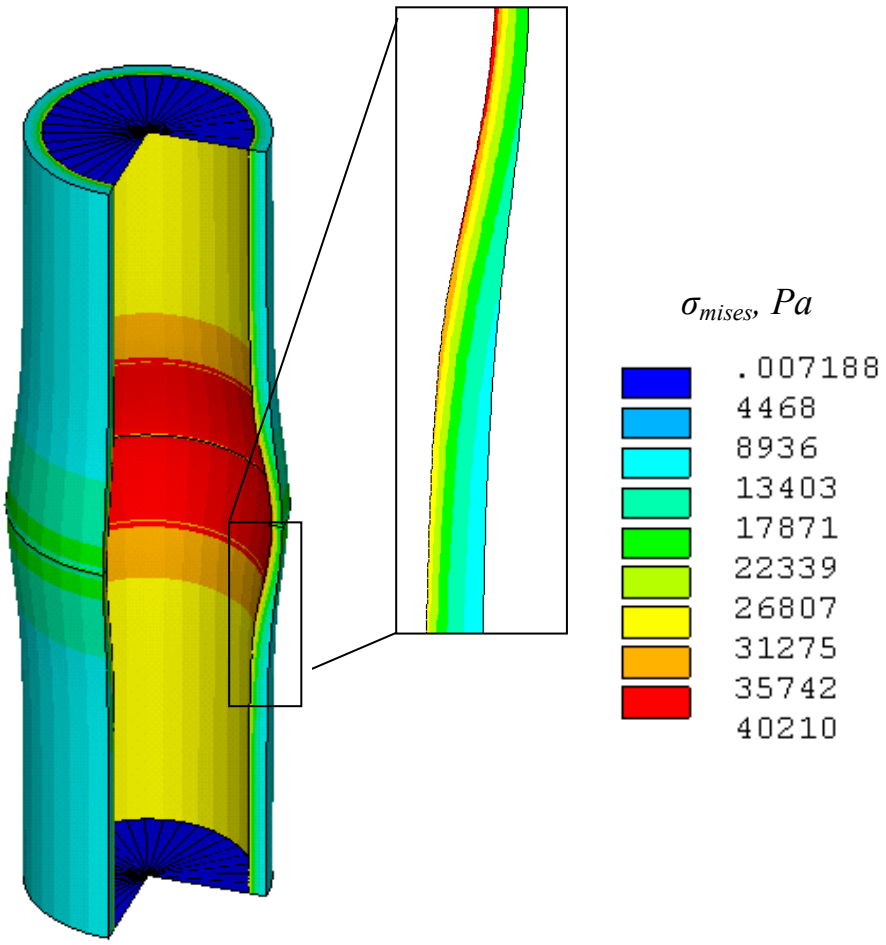

Figure 26. Von Mises stress distribution, corresponding to the moment of collagen recruitment

An important paper dealing with finite element analysis of fusiform aneurysm development has been published by Watton et al [41]. The researchers model the artery tissue as a two-layered material, whereby aneurysms form as a result of time-dependent elastin degradation ("aging"). Such an approach appears to be more realistic than the approach adopted in the current work, which models aneurysm development as a result of increased blood pressure. Implementation of "aging" into the artery tissue model may be one of the directions of future research.

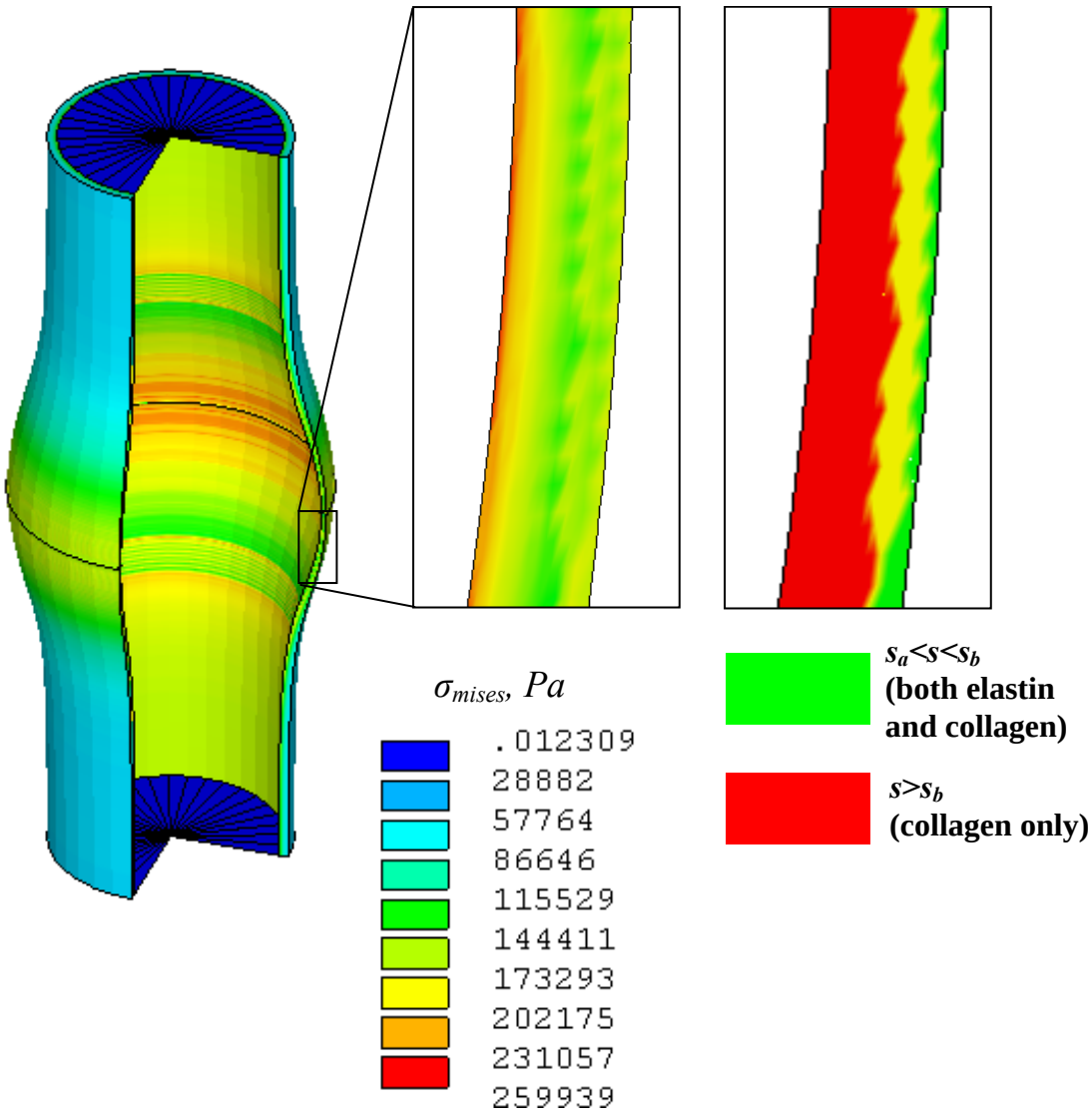

Figure 27. Von Mises stress at the onset of eleastin rupture.
The corresponding distribution of the deformation parameter *s* is shown on the right

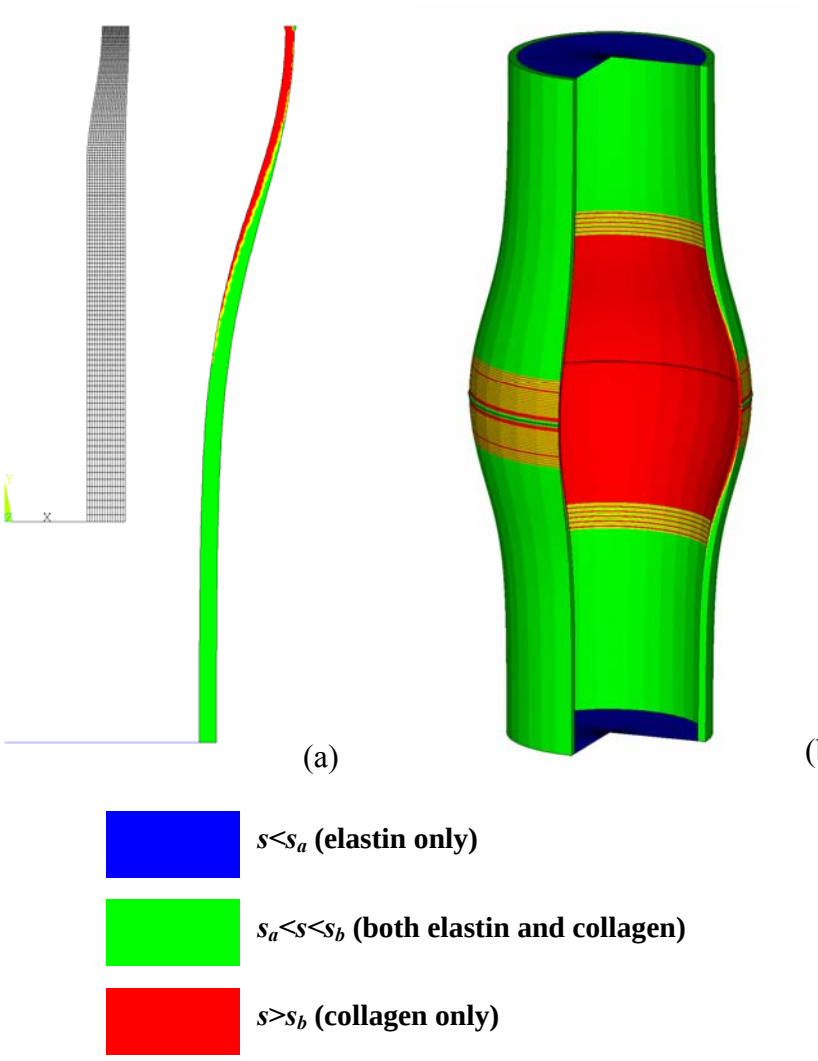

Figure 28. Deformed shape: (a) 2-dimensional; (b) expanded

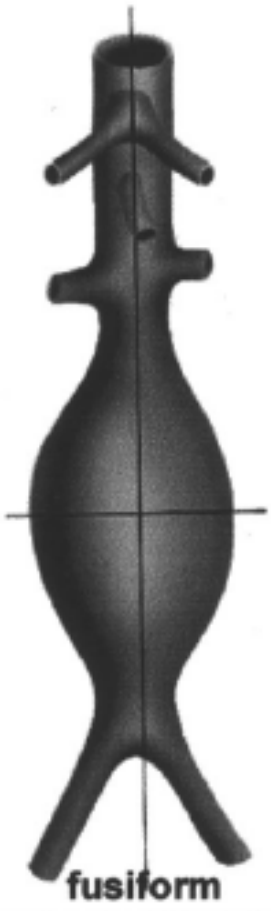

Figure 29. Schematic representation of fusiform aneurysm geometry from [40]

6.0 CONCLUSIONS

In this dissertation, a novel compressible nonlinear multi-mechanism inelastic material model has been introduced for modeling biomechanical tissue, and applied to a numerical study of a procedure of angioplasty, and a process of initiation and development of a fusiform aneurysm. The model was implemented into the commercial finite element software package ANSYS with user programmable features.

This dissertation contains a complete continuum mechanics formulation of the model (inspired by a theoretical work of Wulandana and Robertson [25], and experimental data of Scott et al. [9]), as well as a FORTRAN subroutine, that can be linked to the ANSYS code. The process of the verification of the finite element code is described. The dissertation also includes two computational examples, illustrating how the developed material model can be applied to a numerical simulation of a surgical procedure, and of the development of a vascular disease.

Several major research directions can be recommended for a future development of the proposed material model:

1. Experimental study of the biomechanics of blood vessels;

2. Utilization of the experimental results to answer the question whether anisotropy effects play an important role in the elastic response of vascular tissue, and, if they do, incorporating anisotropy into the model;

3. Utilization of the experimental results to answer the question whether rate effects play an important role in the elastic response of vascular tissue, and, if they do, incorporating viscoelasticity into the model;

4. Utilization of the experimental results to answer the question whether "growth and remodeling" of collagen [24] plays an important role in the elastic response of vascular tissue, and, if they do, incorporating them into the model;

5. Implementation of time-dependent behavior ("aging") into the tissue model.

The significance of the present work relates to the fact that a multi-mechanism inelastic model has never been implemented into a commercial finite element package and applied to a numerical study of physiological processes taking place inside the arterial wall.

It is believed that implementation of the model into a commercial finite element code will assist in the development of surgical treatment of various vascular disorders, and lead to a better understanding of biomechanical properties of vascular tissue.

Additionally, this model can be used for modeling other materials, exhibiting multi-mechanism behavior, such as fiber-reinforced rubbers.

APPENDIX A

SOME IMPORTANT TENSOR ALGEBRA RESULTS

Let us prove some of the identities used in Section 2.

1. Let $\underline{\underline{F}}$ and $\underline{\underline{C}}$ be a deformation gradient and a right Cauchy-Green tensor respectively. Let $J = \det \underline{\underline{F}}$. Calculate the derivative $\dfrac{\partial J}{\partial \underline{\underline{C}}}$.

□

It is well known that

$$\frac{\partial J^2}{\partial \underline{\underline{C}}} = J^2 \underline{\underline{C}}^{-1} \tag{A.1}$$

(c.f. [42]).

Using the chain rule we have

$$\frac{\partial J}{\partial \underline{\underline{C}}} = \frac{\partial J}{\partial J^2}\frac{\partial J^2}{\partial \underline{\underline{C}}} = \frac{1}{2J} J^2 \underline{\underline{C}}^{-1} = \frac{1}{2} J \underline{\underline{C}}^{-1}. \tag{A.2}$$

■

2. Similarly we can use the chain rule to find the derivative $\dfrac{\partial J^{-2/3}}{\partial \underline{\underline{C}}}$:

$$\frac{\partial J^{-2/3}}{\partial \underline{\underline{C}}} = \frac{\partial J^{-2/3}}{\partial J}\frac{\partial J}{\partial \underline{\underline{C}}} = -\frac{2}{3J} J^{-5/3}\frac{1}{2} J \underline{\underline{C}}^{-1} = -\frac{1}{3} J^{-2/3}\underline{\underline{C}}^{-1}. \tag{A.3}$$

3. Let $\overline{\underline{\underline{C}}}$ be a modified right Cauchy-Green tensor: $\underline{\underline{C}} = J^{2/3}\overline{\underline{\underline{C}}}$. Find the derivative $\frac{\partial \overline{\underline{\underline{C}}}}{\partial \underline{\underline{C}}}$.

□

Applying the chain rule we have

$$\frac{\partial \overline{\underline{\underline{C}}}}{\partial \underline{\underline{C}}} = \frac{\partial}{\partial \underline{\underline{C}}}\left(J^{-2/3}\underline{\underline{C}}\right) = \underline{\underline{C}} \otimes \frac{\partial J^{-2/3}}{\partial \underline{\underline{C}}} + J^{-2/3}\,{}^4\underline{\underline{I}} = J^{-2/3}\left({}^4\underline{\underline{I}} - \frac{1}{3}\underline{\underline{C}} \otimes \underline{\underline{C}}^{-1}\right) = J^{-2/3}\,{}^4\underline{\underline{P}}^T, \tag{A.4}$$

where ${}^4\underline{\underline{I}}$ is the fourth order unit tensor, and

$${}^4\underline{\underline{P}} = {}^4\underline{\underline{I}} - \frac{1}{3}\underline{\underline{C}}^{-1} \otimes \underline{\underline{C}} \tag{A.5}$$

is called the *projection tensor*.

■

4. Let $\underline{\underline{A}}$ be the arbitrary second order tensor. Find the derivative $\frac{\partial \underline{\underline{A}}^{-1}}{\partial \underline{\underline{A}}}$.

□

Let us consider the obvious identity

$$\frac{\partial(\underline{\underline{A}}^{-1} \cdot \underline{\underline{A}})}{\partial \underline{\underline{A}}} = {}^4\underline{\underline{O}} \tag{A.6}$$

In indicial notation (A.6) becomes

$$\left(\frac{\partial(\underline{\underline{A}}^{-1} \cdot \underline{\underline{A}})}{\partial \underline{\underline{A}}}\right)_{ijkl} = \frac{\partial A^{-1}_{im}}{\partial A_{kl}} A_{mj} + A^{-1}_{im}\frac{\partial A_{mj}}{\partial A_{kl}} = 0. \tag{A.7}$$

Multiplying the second equation in (A.7) by $\left(\underline{\underline{A}}^{-1}\right)_{jn}$ we have

$$\frac{\partial A^{-1}_{im}}{\partial A_{kl}} A_{mj} A^{-1}_{jn} = -A^{-1}_{im} \frac{\partial A_{mj}}{\partial A_{kl}} A^{-1}_{jn} . \tag{A.8}$$

Further equation (A.8) becomes

$$\frac{\partial A^{-1}_{im}}{\partial A_{kl}} \delta_{mn} = -\frac{1}{2}\left(A^{-1}_{im}\delta_{mk}\delta_{jl}A^{-1}_{jn} + A^{-1}_{im}\delta_{ml}\delta_{jk}A^{-1}_{jn} \right). \tag{A.9}$$

Finally

$$\frac{\partial A^{-1}_{in}}{\partial A_{kl}} = -\frac{1}{2}\left(A^{-1}_{ik}A^{-1}_{\ln} + A^{-1}_{il}A^{-1}_{kn} \right) . \tag{A.10}$$

In Section 3 we used the operation "$\oplus$", which is defined as follows

$$\frac{\partial \underline{\underline{A}}^{-1}}{\partial \underline{\underline{A}}} = -\underline{\underline{A}}^{-1} \oplus \underline{\underline{A}}^{-1} . \tag{A.11}$$

■

5. Prove equation (31).

□

In order to avoid confusion we will omit the index 1.

$$^{4}\underline{\underline{C}}_{vol} = 2\frac{\partial \underline{\underline{S}}_{vol}}{\partial \underline{\underline{C}}} = 2\frac{\partial}{\partial \underline{\underline{C}}}\left(Jp\underline{\underline{C}}^{-1} \right) = 2\left(p\underline{\underline{C}}^{-1} \otimes \frac{1}{2} J\underline{\underline{C}}^{-1} + p\underline{\underline{C}}^{-1} \otimes \frac{\partial p}{\partial J}\frac{1}{2} J\underline{\underline{C}}^{-1} - Jp\underline{\underline{C}}^{-1} \oplus \underline{\underline{C}}^{-1} \right) =$$

$$= J\tilde{p}\underline{\underline{C}}^{-1} \otimes \underline{\underline{C}}^{-1} - 2Jp\underline{\underline{C}}^{-1} \oplus \underline{\underline{C}}^{-1}, \tag{A.12}$$

where $\tilde{p} = p + p\dfrac{\partial p}{\partial J}$.

■

6. Prove equations (33) and (34).

□

Equations (33) and (34) only differ by an index (1 or 2), therefore in the following derivation we will omit the index where possible.

We have

$$ {}^{4}\underline{\underline{\underline{\underline{C}}}}_{1} = 2\frac{\partial \underline{\underline{S}}_{1}}{\partial \underline{\underline{C}}} = 2\frac{\partial}{\partial \underline{\underline{C}}}\left(J^{-2/3}\,{}^{4}\underline{\underline{\underline{\underline{P}}}} : \overline{\underline{\underline{S}}}\right) = 2\frac{\partial}{\partial \underline{\underline{C}}}\left(J^{-2/3}\left(\overline{\underline{\underline{S}}} - \frac{1}{3}\underline{\underline{C}}^{-1}\underline{\underline{C}} : \overline{\underline{\underline{S}}}\right)\right). \tag{A.13} $$

Let us take derivative from each term in (A.13).

From (A.3) we have

$$ \frac{\partial J^{-2/3}}{\partial \underline{\underline{C}}} = -\frac{1}{3}J^{-2/3}\underline{\underline{C}}^{-1}. \tag{A.14} $$

Applying (35) and (A.4) we obtain

$$ \frac{\partial \overline{\underline{\underline{S}}}}{\partial \underline{\underline{C}}} = \frac{\partial \overline{\underline{\underline{S}}}}{\partial \overline{\underline{\underline{C}}}} : \frac{\partial \overline{\underline{\underline{C}}}}{\partial \underline{\underline{C}}} = {}^{4}\overline{\underline{\underline{C}}} : J^{-2/3}\,{}^{4}\underline{\underline{\underline{\underline{P}}}}^{T}. \tag{A.15} $$

Further, applying (35) and (A.11) we obtain

$$ \frac{\partial}{\partial \underline{\underline{C}}}\left(\underline{\underline{C}}^{-1}\underline{\underline{C}} : \overline{\underline{\underline{S}}}\right) = \underline{\underline{C}}^{-1} \otimes \frac{\partial (\underline{\underline{C}} : \overline{\underline{\underline{S}}})}{\partial \overline{\underline{\underline{C}}}} + \underline{\underline{C}} : \overline{\underline{\underline{S}}}\frac{\partial \underline{\underline{C}}^{-1}}{\partial \overline{\underline{\underline{C}}}} = \underline{\underline{C}}^{-1} \otimes \left(J^{2/3}\overline{\underline{\underline{S}}} + \underline{\underline{C}} : {}^{4}\overline{\underline{\underline{C}}}\right) - \underline{\underline{C}} : \overline{\underline{\underline{S}}}\underline{\underline{C}}^{-1} \oplus \underline{\underline{C}}^{-1}. \tag{A.16} $$

Assembling the results (A.14) – (A.16) we have

$$ {}^{4}\underline{\underline{\underline{\underline{C}}}}_{1} = 2\frac{\partial \underline{\underline{S}}_{1}}{\partial \underline{\underline{C}}} $$

$$= -\frac{2}{3}\underline{\underline{S}}_1 \otimes \underline{\underline{C}}^{-1} + \underline{\underline{\underline{\underline{{}^4\overline{C}}}}} : \underline{\underline{\underline{\underline{{}^4P^T}}}} - \frac{2}{3}J^{-2/3}\underline{\underline{C}}^{-1} \otimes \underline{\underline{\overline{S}}} : \underline{\underline{\underline{\underline{{}^4P^T}}}} - \frac{1}{3}\underline{\underline{C}}^{-1} \otimes \underline{\underline{C}} : \underline{\underline{\underline{\underline{{}^4\overline{C}}}}} : \underline{\underline{\underline{\underline{{}^4P^T}}}} + \frac{2}{3}J^{-2/3}\underline{\underline{C}} : \underline{\underline{\overline{S}}}\underline{\underline{C}}^{-1} \oplus \underline{\underline{C}}^{-1} : \underline{\underline{\underline{\underline{{}^4P^T}}}}$$

$$= -\frac{2}{3}\underline{\underline{S}}_1 \otimes \underline{\underline{C}}^{-1} + \underline{\underline{\underline{\underline{{}^4P}}}} : \underline{\underline{\underline{\underline{{}^4\overline{C}}}}} : \underline{\underline{\underline{\underline{{}^4P^T}}}} - \frac{2}{3}J^{-2/3}\underline{\underline{C}}^{-1} \otimes \underline{\underline{\overline{S}}} : \underline{\underline{\underline{\underline{{}^4P^T}}}} + \frac{2}{3}J^{-2/3}\underline{\underline{C}} : \underline{\underline{\overline{S}}}\underline{\underline{C}}^{-1} \oplus \underline{\underline{C}}^{-1} : \left(\underline{\underline{\underline{\underline{{}^4I^T}}}} - \frac{1}{3}\underline{\underline{C}} \otimes \underline{\underline{C}}^{-1}\right)$$

$$= \underline{\underline{\underline{\underline{{}^4P}}}} : \underline{\underline{\underline{\underline{{}^4\overline{C}}}}} : \underline{\underline{\underline{\underline{{}^4P^T}}}} - \frac{2}{3}\left(\underline{\underline{C}}^{-1} \otimes \underline{\underline{S}}_1 + \underline{\underline{S}}_1 \otimes \underline{\underline{C}}^{-1}\right) + \frac{2}{3}J^{-2/3}\underline{\underline{C}} : \underline{\underline{\overline{S}}}\left(\underline{\underline{C}}^{-1} \oplus \underline{\underline{C}}^{-1} - \frac{1}{3}\underline{\underline{C}}^{-1} \otimes \underline{\underline{C}}^{-1}\right) \qquad \text{(A.17)}$$

■

APPENDIX B

EXPRESSIONS FOR STRAIN ENERGY DENSITY FUNCTIONS FOR DIFFERENT HYPERELASTIC MATERIAL MODELS

B.1 NEO-HOOKEAN MATERIAL MODEL

For the Neo-Hookean material model, the strain energy density function is chosen as:

$$\Psi = \frac{\mu}{2}\left(\overline{I}_1 - 3\right) + \frac{1}{d}(J-1)^2 , \tag{B.1}$$

where:

μ is an initial shear modulus;

d is a material incompressibility parameter;

$\overline{I}_1 = tr\overline{\underline{\underline{C}}}$ is the first invariant of the modified right Cauchy-Green deformation tensor $\overline{\underline{\underline{C}}}$;

$J = \sqrt{I_3}$, where $I_3 = \det \underline{\underline{C}}$ is the third invariant of the right Cauchy-Green deformation tensor $\underline{\underline{C}}$.

The initial bulk modulus is related to the material incompressibility parameter by:

$$K = \frac{2}{d} . \tag{B.2}$$

B.2 MOONEY-RIVLIN MATERIAL MODEL

For the Neo-Hookean material model, the strain energy density function is chosen as:

$$\Psi = C_1\left(\overline{I_1} - 3\right) + C_2\left(\overline{I_2} - 3\right) + \frac{1}{d}(J-1)^2, \tag{B.3}$$

where:

C_1, C_2 and d are material parameters;

$\overline{I_1} = tr\overline{\underline{\underline{C}}}$ is the first invariant of the modified right Cauchy-Green deformation tensor $\overline{\underline{\underline{C}}}$;

$\bar{I}_2 = \frac{1}{2}(\mathrm{tr}^2\overline{\underline{\underline{C}}} - \mathrm{tr}\overline{\underline{\underline{C}}}^2)$ is the second invariant of the modified right Cauchy-Green deformation tensor $\overline{\underline{\underline{C}}}$;

$J = \sqrt{I_3}$, where $I_3 = \det\underline{\underline{C}}$ is the third invariant of the right Cauchy-Green deformation tensor $\underline{\underline{C}}$.

Parameter d is also known as a material incompressibility parameter. The initial bulk modulus is related to the material incompressibility parameter by:

$K = \frac{2}{d}$.

B.3 POLYNOMIAL FORM OF THE STRAIN ENERGY DENSITY FUNCTION

For the Polynomial material model, the strain energy density function has the following form:

$$\Psi = \sum_{i+j=1}^{N} C_{ij}\left(\overline{I_1} - 3\right)^i\left(\overline{I_2} - 3\right)^j + \sum_{k=1}^{M}\frac{1}{d_k}(J-1)^{2k}, \tag{B.4}$$

where:

C_{ij} and d_k, *i, j = 1..N, k = 1..M*, are material parameters;

$\overline{I_1} = tr\underline{\underline{\overline{C}}}$ is the first invariant of the modified right Cauchy-Green deformation tensor $\underline{\underline{\overline{C}}}$;

$\bar{\mathrm{I}}_2 = \frac{1}{2}(\mathrm{tr}^2\underline{\underline{\overline{C}}} - \mathrm{tr}\underline{\underline{\overline{C}}}^2)$ is the second invariant of the modified right Cauchy-Green deformation tensor $\underline{\underline{\overline{C}}}$;

$J = \sqrt{I_3}$, where $I_3 = \det\underline{\underline{C}}$ is the third invariant of the right Cauchy-Green deformation tensor $\underline{\underline{C}}$.

B.4 OGDEN FORM OF THE STRAIN ENERGY DENSITY FUNCTION

The Ogden form of strain energy density function is based on the principal stretches, and has the form:

$$\Psi = \sum_{i=1}^{N} \frac{\mu_i}{\alpha_i}\left(\overline{\lambda_1}^{\alpha_i} + \overline{\lambda_2}^{\alpha_i} + \overline{\lambda_3}^{\alpha_i} - 3\right) + \sum_{k=1}^{M} \frac{1}{d_k}(J-1)^{2k} , \qquad \text{(B.5)}$$

where:

μ_i, α_i and d_k, *i = 1..N, k = 1..M*, are material parameters;

λ_1, λ_2 and λ_3 are principal stretches;

$J = \sqrt{I_3}$, where $I_3 = \det\underline{\underline{C}}$ is the third invariant of the right Cauchy-Green deformation tensor $\underline{\underline{C}}$.

B.5 YEOH MATERIAL MODEL

The Yeoh model is also known as the reduced polynomial model. The strain energy function is:

$$\Psi = \sum_{i=1}^{N} c_i (\bar{I}_1 - 3)^i + \sum_{k=1}^{M} \frac{1}{d_k} (J-1)^{2k}, \tag{B.6}$$

where:

c_i and d_k, $i = 1..N$, $k = 1..M$, are material parameters;

$\bar{I}_1 = tr\underline{\underline{\bar{C}}}$ is the first invariant of the modified right Cauchy-Green deformation tensor $\underline{\underline{\bar{C}}}$;

$J = \sqrt{I_3}$, where $I_3 = \det \underline{\underline{C}}$ is the third invariant of the right Cauchy-Green deformation tensor $\underline{\underline{C}}$.

The Neo-Hookean model can be obtained by setting $N = M = 1$.

B.6 EXPONENTIAL HYPERELASTIC MATERIAL MODEL

For the exponential hyperelastic material model the strain energy density function has the following form:

$$\Psi = \alpha \exp\left[\beta\left(\bar{I}_1 - 3\right)\right] + \frac{\alpha\beta}{2}\left(\bar{I}_2 - 3\right) + \frac{1}{d}\left(J-1\right)^2, \tag{B.7}$$

where:

α, β and d are material parameters;

$\bar{I}_1 = tr\underline{\underline{\bar{C}}}$ is the first invariant of the modified right Cauchy-Green deformation tensor $\underline{\underline{\bar{C}}}$;

$\bar{I}_2 = \frac{1}{2}(\mathrm{tr}^2 \underline{\underline{\bar{C}}} - \mathrm{tr}\underline{\underline{\bar{C}}}^2)$ is the second invariant of the modified right Cauchy-Green deformation tensor $\underline{\underline{\bar{C}}}$;

$J = \sqrt{I_3}$, where $I_3 = \det \underline{\underline{C}}$ is the third invariant of the right Cauchy-Green deformation tensor $\underline{\underline{C}}$.

Parameter *d* is also known as a material incompressibility parameter.

B.7 ANISOTROPIC HYPERELASTIC MATERIAL MODEL

In order to define the anisotropic hyperelastic material we need to specify two material directions $\underline{a}$ and $\underline{b}$ (representing directions of the fibers within the tissue). The strain energy density function in this case becomes:

$$\psi(\bar{I}_1, \bar{I}_2, \bar{I}_4, \bar{I}_5, \bar{I}_6, \bar{I}_7, \bar{I}_8, J, \underline{a} \otimes \underline{a}, \underline{b} \otimes \underline{b}) = \sum_{i=1}^{3} a_i (\bar{I}_1 - 3)^i + \sum_{j=1}^{3} b_j (\bar{I}_2 - 3)^j + \sum_{k=2}^{6} c_k (\bar{I}_4 - 1)^k$$
$$+ \sum_{l=2}^{6} d_l (\bar{I}_5 - 1)^l + \sum_{m=2}^{6} e_m (\bar{I}_6 - 1)^m + \sum_{n=2}^{6} f_n (\bar{I}_7 - 1)^n + \sum_{o=2}^{6} g_o (\bar{I}_8 - \varsigma)^o + \frac{1}{d}(J-1)^2 \quad \text{(B.8)}$$

where:

a_i, b_j, c_k, d_l, e_m, f_n, g_o and d, $i = 1..3$, $j = 1..3$, $k = 2..6$, $l = 2..6$, $m = 2..6$, $n = 2..6$, $o = 2..6$, are material parameters;

$\varsigma = (\underline{a} \cdot \underline{b})^2$;

$J = \sqrt{I_3}$, where $I_3 = \det \underline{\underline{C}}$ is the third invariant of the right Cauchy-Green deformation tensor $\underline{\underline{C}}$;

$\bar{I}_1, \bar{I}_2, \bar{I}_4, \bar{I}_5, \bar{I}_6, \bar{I}_7$ and $\bar{I}_8$ are the invariants of the modified right Cauchy-Green deformation tensor $\underline{\underline{\bar{C}}}$, defined as follows:

$\bar{I}_1 = \mathrm{tr}\underline{\underline{\bar{C}}};$
$\bar{I}_2 = \frac{1}{2}(\mathrm{tr}^2\underline{\underline{\bar{C}}} - \mathrm{tr}\underline{\underline{\bar{C}}}^2),$
$\bar{I}_4 = \underline{a} \cdot \underline{\underline{\bar{C}}} \cdot \underline{a},$
$\bar{I}_5 = \underline{a} \cdot \underline{\underline{\bar{C}}}^2 \cdot \underline{a},$
$\bar{I}_6 = \underline{b} \cdot \underline{\underline{\bar{C}}} \cdot \underline{b},$
$\bar{I}_7 = \underline{b} \cdot \underline{\underline{\bar{C}}}^2 \cdot \underline{b},$
$\bar{I}_8 = (\underline{a} \cdot \underline{b})\underline{a} \cdot \underline{\underline{\bar{C}}} \cdot \underline{b}$

Parameter *d* is also known as a material incompressibility parameter.

B.8 HEART TISSUE MATERIAL MODEL IN LS-DYNA

This material model is based on the formulation of [22], and is described by the strain energy density function in terms of the components of the Green strain as follows:

$$\Psi = \frac{C}{2}\left(e^{Q} - 1\right) + \frac{1}{d}(J-1)^2, \tag{B.9}$$

where:

$Q = b_1 E_{11}^2 + b_2\left(E_{22}^2 + E_{33}^2 + E_{23}^2 + E_{32}^2\right) + b_3\left(E_{12}^2 + E_{21}^2 + E_{13}^2 + E_{31}^2\right);$

E_{ij}, $i,j = 1..3$, are the Green strain components;

C, b_1, b_2, b_3 and d are material parameters (parameter d is also known as a material incompressibility parameter);

$J = \sqrt{I_3}$, where $I_3 = \det \underline{\underline{C}}$ is the third invariant of the right Cauchy-Green deformation tensor $\underline{\underline{C}}$.

B.9 ISOTROPIC LUNG TISSUE MATERIAL MODEL IN LS-DYNA

This material model is based on the formulation of [23], and is described by the strain energy density function of the following form:

$$\Psi = \frac{C}{2\Delta} e^{\left(\alpha I_1^2 + \beta I_2\right)} + \frac{12C_1}{\Delta(1+C_2)}(A^{(1+C_2)} - 1) + \frac{1}{d}(J-1)^2, \tag{B.10}$$

where:

$A^2 = \frac{4}{3}(I_1 + I_2) - 1$;

Δ, C, C_1, C_2 and d are material parameters;

$\overline{I_1} = tr\overline{\underline{\underline{C}}}$ is the first invariant of the modified right Cauchy-Green deformation tensor $\overline{\underline{\underline{C}}}$;

$\bar{I}_2 = \frac{1}{2}(\mathrm{tr}^2 \overline{\underline{\underline{C}}} - \mathrm{tr}\overline{\underline{\underline{C}}}^2)$ is the second invariant of the modified right Cauchy-Green deformation tensor $\overline{\underline{\underline{C}}}$;

$J = \sqrt{I_3}$, where $I_3 = \det \underline{\underline{C}}$ is the third invariant of the right Cauchy-Green deformation tensor $\underline{\underline{C}}$.

Parameter d is also known as a material incompressibility parameter.

APPENDIX C

USERMAT3D FORTRAN CODE

```
      subroutine usermat3d(
     &                    matId, elemId,kDomIntPt, kLayer, kSectPt,
     &                    ldstep,isubst,keycut,
     &                    nDirect,nShear,ncomp,nStatev,nProp,
     &                    Time,dTime,Temp,dTemp,
     &                    stress,ustatev,dsdePl,sedEl,sedPl,epseq,
     &                    Strain,dStrain, epsPl, prop, coords,
     &                    rotateM, defGrad_t, defGrad,
     &                    tsstif, epsZZ,
     &                    var1, var2, var3, var4, var5,
     &                    var6, var7, var8)
c**********************************************************************
c
c     input arguments
c     ===============
c      matId     (int,sc,i)              material #
c      elemId    (int,sc,i)              element #
c      kDomIntPt (int,sc,i)              "k"th domain integration point
c      kLayer    (int,sc,i)              "k"th layer
c      kSectPt   (int,sc,i)              "k"th Section point
c      ldstep    (int,sc,i)              load step number
c      isubst    (int,sc,i)              substep number
c      nDirect   (int,sc,in)             # of direct components
c      nShear    (int,sc,in)             # of shear components
c      ncomp     (int,sc,in)             nDirect + nShear
c      nstatev   (int,sc,l)              Number of state variables
c      nProp     (int,sc,l)              Number of material ocnstants
c
c      Temp      (dp,sc,in)              temperature at beginning of
c                                        time increment
c      dTemp     (dp,sc,in)              temperature increment
c      Time      (dp,sc,in)              time at beginning of increment (t)
c      dTime     (dp,sc,in)              current time increment (dt)
c
c      Strain   (dp,ar(ncomp),i)         Strain at beginning of time
c                                                              increment
c      dStrain  (dp,ar(ncomp),i)         Strain increment
```

```
c      prop     (dp,ar(nprop),i)          Material constants defined by
c                                                                  TB,USER
c      coords   (dp,ar(3),i)              current coordinates
c      rotateM  (dp,ar(3,3),i)            Rotation matrix for finite
c                                                        deformation update
c                                         Used only in 5.6 and 5.7
c                                         Unit matrix in 6.0 and late version
c      defGrad_t(dp,ar(3,3),i)            Deformation gradient at time t
c      defGrad  (dp,ar(3,3),i)            Deformation gradient at time t+dt
c
c     input output arguments
c     ======================
c      stress   (dp,ar(nTesn),io)         stress
c      ustatev   (dp,ar(nstatev),io)      user state variable
c            ustatev(1)                     - equivalent plastic strain
c            ustatev(2) - statev(1+ncomp)   - plastic strain vector
c            ustatev(nStatev)               - von-Mises stress
c      sedEl    (dp,sc,io)                elastic work
c      sedPl    (dp,sc,io)                plastic work
c      epseq    (dp,sc,io)                equivalent plastic strain
c      tsstif   (dp,ar(2),io)             transverse shear stiffness
c                                         tsstif(1) - Gxz
c                                         tsstif(2) - Gyz
c                                         tsstif(1) is also used to calculate
c                                                                  hourglass
c                                         stiffness, this value must be
c                                                        defined when low
c                                         order element, such as 181, 182,
c                                                        185 with uniform
c                                         integration is used.
c      var?     (dp,sc,io)                not used, they are reserved
c                                                                  arguments
c                                         for further development
c
c     output arguments
c     ================
c      keycut   (int,sc,io)               loading bisect/cut control
c                                         0 - no bisect/cut
c                                         1 - bisect/cut
c                                         (factor will be determined by ANSYS
c                                                      solution control)
c      dsdePl   (dp,ar(ncomp,ncomp),io)   material jacobian matrix
c      epsZZ    (dp,sc,o)                 strain epsZZ for plane stress,
c                                         define it when accounting for
c                                                       thickness change
c                                         in shell and plane stress states
c
c*********************************************************************
c
c      ncomp   6   for 3D  (nshear=3)
c      ncomp   4   for plane strain or axisymmetric (nShear = 1)
c      ncomp   3   for plane stress (nShear = 1)
c      ncomp   3   for 3d beam      (nShear = 2)
c      ncomp   1   for 1D (nShear = 0)
c
c      stresss and strains, plastic strain vectors
c          11, 22, 33, 12, 23, 13    for 3D
```

```
c          11, 22, 33, 12           for plane strain or axisymmetry
c          11, 22, 12               for plane stress
c          11, 13, 12               for 3d beam
c          11                       for 1D
c
c      material jacobian matrix
c        3D
c           dsdePl    |  1111   1122   1133   1112   1123   1113 |
c           dsdePl    |  2211   2222   2233   2212   2223   2213 |
c           dsdePl    |  3311   3322   3333   3312   3323   3313 |
c           dsdePl    |  1211   1222   1233   1212   1223   1213 |
c           dsdePl    |  2311   2322   2333   2312   2323   2313 |
c           dsdePl    |  1311   1322   1333   1312   1323   1313 |
c        plane strain or axisymmetric (11, 22, 33, 12)
c           dsdePl    |  1111   1122   1133   1112 |
c           dsdePl    |  2211   2222   2233   2212 |
c           dsdePl    |  3311   3322   3333   3312 |
c           dsdePl    |  1211   1222   1233   1212 |
c        plane stress (11, 22, 12)
c           dsdePl    |  1111   1122   1112 |
c           dsdePl    |  2211   2222   2212 |
c           dsdePl    |  1211   1222   1212 |
c        3d beam (11, 13, 12)
c           dsdePl    |  1111   1113   1112 |
c           dsdePl    |  1311   1313   1312 |
c           dsdePl    |  1211   1213   1212 |
c        1d
c           dsdePl    |  1111 |
c
c**********************************************************************
#include "impcom.inc"
c
      INTEGER
     &                 matId, elemId,
     &                 kDomIntPt, kLayer, kSectPt,
     &                 ldstep,isubst,keycut,
     &                 nDirect,nShear,ncomp,nStatev,nProp
      DOUBLE PRECISION
     &                 Time,    dTime,   Temp,    dTemp,
     &                 sedEl,   sedPl,   epseq,   epsZZ
      DOUBLE PRECISION
     &                 stress  (ncomp  ), ustatev (nStatev),
     &                 dsdePl  (ncomp,ncomp),
     &                 Strain  (ncomp  ), dStrain (ncomp  ),
     &                 epsPl   (ncomp  ), prop    (nProp  ),
     &                 coords  (3),       rotateM (3,3),
     &                 defGrad (3,3),     defGrad_t(3,3),
     &                 tsstif  (2)
c
c***************** User defined part **********************************
c
c --- functions
c
      DOUBLE PRECISION DoubleDot,det,delta,Trace
c
c --- local variables
c
```

```
c Scalars
      DOUBLE PRECISION JJ,alpha1,alpha2,gamma1,gamma2,sa,sb,
     & s,d,I1,I2,JJ2,Jsa,p,ptilda
c 2nd order tensors
      DOUBLE PRECISION Identity(3,3),FT(3,3),FBar(3,3),
     & FBarT(3,3),C(3,3),Cinv(3,3),CBar(3,3),SigmaVol(3,3),
     & SBar(3,3),T1(3,3),Siso(3,3),SigmaIsoVoight(3,3),
     & SigmaIso(3,3),Fsa(3,3),FsaInv(3,3),F2(3,3),C2(3,3),F2t(3,3),
     & C2inv(3,3),FsaBar(3,3),FsaBarInv(3,3),
     & FsaBarInvT(3,3),C2Bar(3,3),SBar1(3,3),Siso1(3,3),
     & SigmaIso1(3,3),SigmaIsoVoight1(3,3),SBar2(3,3),Siso2(3,3),
     & SigmaIso2(3,3),SigmaIsoVoight2(3,3)
c 4th order tensors
      DOUBLE PRECISION II(3,3,3,3),Cref(3,3,3,3),Cspac(3,3,3,3),
     & Cref1(3,3,3,3),Cspac1(3,3,3,3),Cref2(3,3,3,3),Cspac2(3,3,3,3),
     & CC(3,3,3,3),CCC(3,3,3,3),Cvol(3,3,3,3),TT1(3,3,3,3),TT2(3,3,3,3)
c
c
      DOUBLE PRECISION var1, var2, var3, var4, var5,
     &                 var6, var7, var8
      INTEGER          i,j,k,l,m,IO,ic,jc,kc,lc
c
c**********************************************************************
c
c Form identity matrix
      do i=1,3
       do j=1,3
        Identity(i,j)=delta(i,j)
       end do
      end do
c Input material parameters
      alpha1=prop(1)
      alpha2=prop(2)
      gamma1=prop(3)
      gamma2=prop(4)
      sa=prop(5)
      sb=prop(6)
      d=prop(7)
c Calculate determinant of defGrad
      JJ=det(defGrad)
c Calculate right Cauchy-Green deformation tensor
      call Transpose(FT,DefGrad)
      call MulTens(C,FT,DefGrad,1.0d0)
c Calculate C-inverse
      call Inverse(Cinv,C,1.0d0)
c Calculate the barred values
      call ScalTensor(FBar,defGrad,JJ**(-1.0d0/3.0d0))
      call Transpose(FBarT,FBar)
      call ScalTensor(CBar,C,JJ**(-2.0d0/3.0d0))
c Calculate the invariants
      call MulTens(T1,CBar,CBar,1.0d0)
      I1=Trace(CBar)
c Calculate volumetric part of Cauchy stress and elastic tensor
      p=2.0d0/d*(JJ-1.0d0)
      ptilda=2.0d0/d*(2.0d0*JJ-1.0d0)
      call ScalTensor(SigmaVol,Identity,p)
      call TensorProduct(TT1,Cinv,Cinv,JJ*ptilda)
```

```
      call WheelProduct(TT2,Cinv,-2.0d0*p*JJ)
      call AddTens4(CVol,TT1,TT2)
c Deformation state parameter
      s=I1-3.0d0
      ustatev(11)=s
c Determine active deformation mechanism
      IF (s.LT.sa) THEN
       if (ustatev(10).ne.0) ustatev(10)=0
       call GetStress(IO,alpha1,gamma1,I1,JJ,C,Cinv,defGrad,FT,
     & SigmaIsoVoight,SigmaIso,Siso,SBar)
c *********************************************************
       call GetStiffness(IO,alpha1,gamma1,I1,JJ,C,Cinv,defGrad,Siso,
     & SBar,Cref,Cspac)
      ELSE
c Second or third deformation mechanism
       if (ustatev(10).eq.0) then
        IF (s.LT.sb) ustatev(10) = 1
        if (s.ge.sb) ustatev(10) = 2
        call ScalTensor(Fsa,defGrad_t,1.0d0)
        ustatev(1)=Fsa(1,1)
        ustatev(2)=Fsa(1,2)
        ustatev(3)=Fsa(1,3)
        ustatev(4)=Fsa(2,1)
        ustatev(5)=Fsa(2,2)
        ustatev(6)=Fsa(2,3)
        ustatev(7)=Fsa(3,1)
        ustatev(8)=Fsa(3,2)
        ustatev(9)=Fsa(3,3)
       else
        Fsa(1,1)=ustatev(1)
        Fsa(1,2)=ustatev(2)
        Fsa(1,3)=ustatev(3)
        Fsa(2,1)=ustatev(4)
        Fsa(2,2)=ustatev(5)
        Fsa(2,3)=ustatev(6)
        Fsa(3,1)=ustatev(7)
        Fsa(3,2)=ustatev(8)
        Fsa(3,3)=ustatev(9)
       end if
       Jsa=det(Fsa)
       call Inverse(FsaInv,Fsa,1.0d0)
       call MulTens(F2,defGrad,FsaInv,1.0d0)
       call Transpose(F2t,F2)
       call MulTens(C2,F2t,F2,1.0d0)
       JJ2=det(F2)
       call Inverse(C2Inv,C2,1.0d0)
       call ScalTensor(FsaBar,Fsa,Jsa**(-1.0d0/3.0d0))
       call Inverse(FsaBarInv,FsaBar,1.0d0)
       call Transpose(FsaBarInvT,FsaBarInv)
       call MulTens(T1,FsaBarInvT,CBar,1.0d0)
       call MulTens(C2Bar,T1,FsaBarInv,1.0d0)
       I2=Trace(C2Bar)
       IF (s.GE.sb) THEN
c Third deformation mechanism
        ustatev(10) = 2
        call GetStress(IO,alpha2,gamma2,I2,JJ2,C2,C2inv,F2,F2t,
     & SigmaIsoVoight,SigmaIso,Siso,SBar)
```

```
         call GetStiffness(IO,alpha2,gamma2,I2,JJ2,C2,C2inv,F2,Siso,
     & SBar,Cref,Cspac)
        ELSE
c Second deformation mechanism
         ustatev(10) = 1
         call GetStress(IO,alpha1,gamma1,I1,JJ,C,Cinv,defGrad,FT,
     & SigmaIsoVoight1,SigmaIso1,Siso1,SBar1)
         call GetStiffness(IO,alpha1,gamma1,I1,JJ,C,Cinv,defGrad,Siso1,
     & SBar1,Cref1,Cspac1)
         call GetStress(IO,alpha2,gamma2,I2,JJ2,C2,C2inv,F2,F2t,
     & SigmaIsoVoight2,SigmaIso2,Siso2,SBar2)
         call GetStiffness(IO,alpha2,gamma2,I2,JJ2,C2,C2inv,F2,Siso2,
     & SBar2,Cref2,Cspac2)
         call AddTensSc(SigmaIso,SigmaIso1,SigmaIso2,1.0d0,1.0d0)
         call AddTens4(Cspac,Cspac1,Cspac2)
        END IF
       END IF
c Form output stress vector
       stress(1)=SigmaVol(1,1)+SigmaIso(1,1)
       stress(2)=SigmaVol(2,2)+SigmaIso(2,2)
       stress(3)=SigmaVol(3,3)+SigmaIso(3,3)
       stress(4)=SigmaVol(1,2)+SigmaIso(1,2)
       IF (ncomp.eq.6) THEN
        stress(5)=SigmaVol(2,3)+SigmaIso(2,3)
        stress(6)=SigmaVol(1,3)+SigmaIso(1,3)
       END IF
c Calculate spatial volumetric tangent moduli (push-forward)
       do i=1,3
         do j=1,3
           do k=1,3
             do l=1,3
               CC(i,j,k,l)=0.0d0
               do ic=1,3
                 do jc=1,3
                   do kc=1,3
                     do lc=1,3
                       CC(i,j,k,l)=CC(i,j,k,l)+
     & defGrad(i,ic)*defGrad(j,jc)*defGrad(k,kc)*defGrad(l,lc)*
     & CVol(ic,jc,kc,lc)/JJ
                     end do
                   end do
                 end do
               end do
             end do
           end do
         end do
       end do
c Update stiffness
       call AddTens4(CCC,Cspac,CC)
       dsdePl(1,1)=CCC(1,1,1,1)
       dsdePl(1,2)=CCC(1,1,2,2)
       dsdePl(1,3)=CCC(1,1,3,3)
       dsdePl(1,4)=CCC(1,1,1,2)
       dsdePl(2,1)=CCC(2,2,1,1)
       dsdePl(2,2)=CCC(2,2,2,2)
       dsdePl(2,3)=CCC(2,2,3,3)
       dsdePl(2,4)=CCC(2,2,1,2)
```

```
      dsdePl(3,1)=CCC(3,3,1,1)
      dsdePl(3,2)=CCC(3,3,2,2)
      dsdePl(3,3)=CCC(3,3,3,3)
      dsdePl(3,4)=CCC(3,3,1,2)
      dsdePl(4,1)=CCC(1,2,1,1)
      dsdePl(4,2)=CCC(1,2,2,2)
      dsdePl(4,3)=CCC(1,2,3,3)
      dsdePl(4,4)=CCC(1,2,1,2)
      IF (ncomp.eq.6) THEN
       dsdePl(5,1)=CCC(2,3,1,1)
       dsdePl(5,2)=CCC(2,3,2,2)
       dsdePl(5,3)=CCC(2,3,3,3)
       dsdePl(5,4)=CCC(2,3,1,2)
       dsdePl(5,5)=CCC(2,3,2,3)
       dsdePl(5,6)=CCC(2,3,1,3)
       dsdePl(6,1)=CCC(1,3,1,1)
       dsdePl(6,2)=CCC(1,3,2,2)
       dsdePl(6,3)=CCC(1,3,3,3)
       dsdePl(6,4)=CCC(1,3,1,2)
       dsdePl(6,5)=CCC(1,3,2,3)
       dsdePl(6,6)=CCC(1,3,1,3)
       dsdePl(1,5)=CCC(1,1,2,3)
       dsdePl(1,6)=CCC(1,1,1,3)
       dsdePl(2,5)=CCC(2,2,2,3)
       dsdePl(2,6)=CCC(2,2,1,3)
       dsdePl(3,5)=CCC(3,3,2,3)
       dsdePl(3,6)=CCC(3,3,1,3)
       dsdePl(4,5)=CCC(1,2,2,3)
       dsdePl(4,6)=CCC(1,2,1,3)
      END IF
c That's all folks
      return
      end
c *********************************************************************
      SUBROUTINE MULTENS(TensRes,Tens1,Tens2,fact)
      DOUBLE PRECISION TensRes(3,3),Tens1(3,3),Tens2(3,3),fact
      INTEGER i,j,k
      do i=1,3
        do j=1,3
          TensRes(i,j)=0.0d0
          do k=1,3
            TensRes(i,j)=TensRes(i,j)+Tens1(i,k)*Tens2(k,j)
          end do
          TensRes(i,j)=TensRes(i,j)*fact
        end do
      end do
      END
c
      SUBROUTINE WheelProduct(TensRes,Tens1,fact)
      DOUBLE PRECISION TensRes(3,3,3,3),Tens1(3,3),fact
      INTEGER i,j,k,l
      do i=1,3
        do j=1,3
          do k=1,3
            do l=1,3
              TensRes(i,j,k,l)=fact/2.0d0*(Tens1(i,k)*Tens1(j,l)+
     & Tens1(i,l)*Tens1(j,k))
```

```
            end do
          end do
        end do
      end do
      END
c
      SUBROUTINE TensorProduct(TensRes,Tens1,Tens2,fact)
      DOUBLE PRECISION TensRes(3,3,3,3),Tens1(3,3),Tens2(3,3),fact
      INTEGER i,j,k,l
      do i=1,3
        do j=1,3
          do k=1,3
           do l=1,3
            TensRes(i,j,k,l)=fact*Tens1(i,j)*Tens2(k,l)
           end do
          end do
        end do
      end do
      END
c
      SUBROUTINE ScalTensor(TensRes,Tensr,fact)
      DOUBLE PRECISION TensRes(3,3),Tensr(3,3),fact
      INTEGER i,j
      do i=1,3
        do j=1,3
          TensRes(i,j)=Tensr(i,j)*fact
        end do
      end do
      END
c
      SUBROUTINE ScalTens4(TensRes,Tensr,fact)
      DOUBLE PRECISION TensRes(3,3,3,3),Tensr(3,3,3,3),fact
      INTEGER i,j,k,l
      do i=1,3
        do j=1,3
          do k=1,3
            do l=1,3
              TensRes(i,j,k,l)=Tensr(i,j,k,l)*fact
            end do
          end do
        end do
      end do
      END
c
      Function DoubleDot(Tens1,Tens2)
      DOUBLE PRECISION Tens1(3,3),Tens2(3,3),DoubleDot
      INTEGER i,j
      DoubleDot=0.0d0
      do i=1,3
        do j=1,3
          DoubleDot=DoubleDot+Tens1(i,j)*Tens2(i,j)
        end do
      end do
      return
      END
c
      SUBROUTINE DoubleDot4(C,A,B,fact)
```

```
      DOUBLE PRECISION A(3,3,3,3),B(3,3,3,3),C(3,3,3,3)
      DOUBLE PRECISION fact
      INTEGER i,j,k,l,m,n
      do i=1,3
        do j=1,3
          do k=1,3
            do l=1,3
              C(i,j,k,l)=0.0d0
              do m=1,3
                do n=1,3
                  C(i,j,k,l)=C(i,j,k,l)+fact*A(i,j,m,n)*B(m,n,k,l)
                end do
              end do
            end do
          end do
        end do
      end do
      END
c
      SUBROUTINE T4ddT2(Tres,T4,T2,fact)
      DOUBLE PRECISION T4(3,3,3,3),T2(3,3),Tres(3,3)
      DOUBLE PRECISION fact
      INTEGER i,j,k,l
      do i=1,3
        do j=1,3
          Tres(i,j)=0.0d0
          do k=1,3
            do l=1,3
              Tres(i,j)=Tres(i,j)+fact*T4(i,j,k,l)*T2(k,l)
            end do
          end do
        end do
      end do
      END
c
      SUBROUTINE T2ddT4(Tres,T2,T4,fact)
      DOUBLE PRECISION T4(3,3,3,3),T2(3,3),Tres(3,3)
      DOUBLE PRECISION fact
      INTEGER i,j,k,l
      do i=1,3
        do j=1,3
          Tres(i,j)=0.0d0
          do k=1,3
            do l=1,3
              Tres(i,j)=Tres(i,j)+fact*T4(k,l,i,j)*T2(k,l)
            end do
          end do
        end do
      end do
      END
c
      Function Trace(Tensor)
      DOUBLE PRECISION Tensor(3,3),Trace
      INTEGER i
      Trace=0.0d0
      do i=1,3
        Trace=Trace+Tensor(i,i)
```

```
      end do
      return
      END
c
      SUBROUTINE Transpose(TensRes,Tensor)
      DOUBLE PRECISION TensRes(3,3),Tensor(3,3)
      INTEGER i,j
      do i=1,3
        do j=1,3
          TensRes(i,j)=Tensor(j,i)
        end do
      end do
      END
c
      SUBROUTINE DEV(TensRes,Tensor)
      DOUBLE PRECISION TensRes(3,3),Tensor(3,3),p
      p=Tensor(1,1)+Tensor(2,2)+Tensor(3,3)
      TensRes(1,1)=Tensor(1,1)-p/3.0d0
      TensRes(3,3)=Tensor(3,3)-p/3.0d0
      TensRes(2,2)=Tensor(2,2)-p/3.0d0
      TensRes(1,2)=Tensor(1,2)
      TensRes(2,1)=Tensor(2,1)
      TensRes(3,1)=Tensor(3,1)
      TensRes(1,3)=Tensor(1,3)
      TensRes(2,3)=Tensor(2,3)
      TensRes(3,2)=Tensor(3,2)
      END
c
      SUBROUTINE EquateTens(Tens1,Tens2)
      DOUBLE PRECISION Tens1(3,3),Tens2(3,3)
      INTEGER i,j
      do i=1,3
        do j=1,3
          Tens1(i,j)=Tens2(i,j)
        end do
      end do
      END
c
      SUBROUTINE ADDTENSSC(TensRes,Tens1,Tens2,fact1,fact2)
      DOUBLE PRECISION TensRes(3,3),Tens1(3,3),Tens2(3,3),fact1,fact2
      INTEGER i,j
      do i=1,3
        do j=1,3
          TensRes(i,j)=Tens1(i,j)*fact1+Tens2(i,j)*fact2
        end do
      end do
      END
c
      SUBROUTINE ADDTENS4(TensRes,Tens1,Tens2)
      DOUBLE PRECISION TensRes(3,3,3,3),Tens1(3,3,3,3),Tens2(3,3,3,3)
      INTEGER i,j,k,l
      do i=1,3
        do j=1,3
          do k=1,3
            do l=1,3
              TensRes(i,j,k,l)=Tens1(i,j,k,l)+Tens2(i,j,k,l)
            end do
```

```
          end do
        end do
      end do
      END
c
      FUNCTION delta(i,j)
      DOUBLE PRECISION delta
      INTEGER i,j
      IF (i.eq.j) delta=1.0d0
      IF (i.ne.j) delta=0.0d0
      RETURN
      END
c
      FUNCTION det(T)
      DOUBLE PRECISION det,T(3,3)
      det=T(1,1)*T(2,2)*T(3,3)+T(2,1)*T(3,2)*T(1,3)+T(1,2)*T(2,3)*T(3,1)
     & -T(1,2)*T(2,1)*T(3,3)-T(2,3)*T(3,2)*T(1,1)-T(3,1)*T(2,2)*T(1,3)
      RETURN
      END
c Returns Inverse of the matrix
      SUBROUTINE Inverse(TensRes,Tensr,fact)
      DOUBLE PRECISION TensRes(3,3),Tensr(3,3),fact,d,det
      INTEGER i,j
      TensRes(1,1)=Tensr(2,2)*Tensr(3,3)-Tensr(2,3)*Tensr(3,2)
      TensRes(1,2)=Tensr(1,3)*Tensr(3,2)-Tensr(3,3)*Tensr(1,2)
      TensRes(1,3)=Tensr(1,2)*Tensr(2,3)-Tensr(2,2)*Tensr(1,3)
      TensRes(2,1)=Tensr(2,3)*Tensr(3,1)-Tensr(3,3)*Tensr(2,1)
      TensRes(2,2)=Tensr(1,1)*Tensr(3,3)-Tensr(1,3)*Tensr(3,1)
      TensRes(2,3)=Tensr(1,3)*Tensr(2,1)-Tensr(2,3)*Tensr(1,1)
      TensRes(3,1)=Tensr(2,1)*Tensr(3,2)-Tensr(2,2)*Tensr(3,1)
      TensRes(3,2)=Tensr(1,2)*Tensr(3,1)-Tensr(1,1)*Tensr(3,2)
      TensRes(3,3)=Tensr(2,2)*Tensr(1,1)-Tensr(2,1)*Tensr(1,2)
      d=det(Tensr)
      do j=1,3
        do i=1,3
          TensRes(i,j)=TensRes(i,j)*fact/d
        end do
      end do
      return
      end
c
      SUBROUTINE Voight(Tss,Ttttt)
      Double Precision Tss(6,6),Ttttt(3,3,3,3)
      Tss(1,1)=Ttttt(1,1,1,1)
      Tss(1,2)=Ttttt(1,1,2,2)
      Tss(1,3)=Ttttt(1,1,3,3)
      Tss(1,4)=Ttttt(1,1,1,2)
      Tss(1,5)=Ttttt(1,1,2,3)
      Tss(1,6)=Ttttt(1,1,1,3)
      Tss(2,1)=Ttttt(2,2,1,1)
      Tss(2,2)=Ttttt(2,2,2,2)
      Tss(2,3)=Ttttt(2,2,3,3)
      Tss(2,4)=Ttttt(2,2,1,2)
      Tss(2,5)=Ttttt(2,2,2,3)
      Tss(2,6)=Ttttt(2,2,1,3)
      Tss(3,1)=Ttttt(3,3,1,1)
      Tss(3,2)=Ttttt(3,3,2,2)
```

```
      Tss(3,3)=Ttttt(3,3,3,3)
      Tss(3,4)=Ttttt(3,3,1,2)
      Tss(3,5)=Ttttt(3,3,2,3)
      Tss(3,6)=Ttttt(3,3,1,3)
      Tss(4,1)=Ttttt(1,2,1,1)
      Tss(4,2)=Ttttt(1,2,2,2)
      Tss(4,3)=Ttttt(1,2,3,3)
      Tss(4,4)=Ttttt(1,2,1,2)
      Tss(4,5)=Ttttt(1,2,2,3)
      Tss(4,6)=Ttttt(1,2,1,3)
      Tss(5,1)=Ttttt(2,3,1,1)
      Tss(5,2)=Ttttt(2,3,2,2)
      Tss(5,3)=Ttttt(2,3,3,3)
      Tss(5,4)=Ttttt(2,3,1,2)
      Tss(5,5)=Ttttt(2,3,2,3)
      Tss(5,6)=Ttttt(2,3,1,3)
      Tss(6,1)=Ttttt(1,3,1,1)
      Tss(6,2)=Ttttt(1,3,2,2)
      Tss(6,3)=Ttttt(1,3,3,3)
      Tss(6,4)=Ttttt(1,3,1,2)
      Tss(6,5)=Ttttt(1,3,2,3)
      Tss(6,6)=Ttttt(1,3,1,3)
      end
c *****************************************************************
      SUBROUTINE GetStress(IO,alpha,gamma,I,JJ,C,Cinv,F,FT,
     & SigmaIsoVoight,SigmaIso,Siso,SBar)
      DOUBLE PRECISION alpha,gamma,I,JJ,aaa,delta,DoubleDot
      DOUBLE PRECISION C(3,3),Cinv(3,3),SigmaIso(3,3),SigmaIsoVoight(6),
     & Siso(3,3),Sbar(3,3),T1(3,3),T2(3,3),F(3,3),FT(3,3),Identity(3,3)
      INTEGER ic,j,IO
c Form identity matrix
      do ic=1,3
       do j=1,3
        Identity(ic,j)=delta(ic,j)
       end do
      end do
c Calculate SBar
      aaa=alpha*exp(gamma*(I-3.0d0))
      call ScalTensor(SBar,Identity,aaa)
c Calculate Siso
      call ScalTensor(T1,Sbar,JJ**(-2.0d0/3.0d0))
      aaa=-JJ**(-2.0d0/3.0d0)/3.0d0*DoubleDot(C,Sbar)
      call ScalTensor(T2,Cinv,aaa)
      call AddTensSc(Siso,T1,T2,1.0d0,1.0d0)
c Calculate SigmaIso
      call MulTens(T1,F,Siso,JJ**(-1.0d0))
      call MulTens(SigmaIso,T1,FT,1.0d0)
c Form output stress vector
      SigmaIsoVoight(1)=SigmaIso(1,1)
      SigmaIsoVoight(2)=SigmaIso(2,2)
      SigmaIsoVoight(3)=SigmaIso(3,3)
      SigmaIsoVoight(4)=SigmaIso(1,2)
      SigmaIsoVoight(5)=SigmaIso(2,3)
      SigmaIsoVoight(6)=SigmaIso(1,3)
      END
c *****************************************************************
      SUBROUTINE GetStiffness(IO,alpha,gamma,II,JJ,C,Cinv,F,Siso,SBar,
```

```
     & Cref,Cspac)
      DOUBLE PRECISION alpha,gamma,II,JJ,aaa,bbb,delta,DoubleDot
      DOUBLE PRECISION C(3,3),Cinv(3,3),Siso(3,3),Sbar(3,3),
     & T21(3,3),T22(3,3),F(3,3),Identity(3,3)
      DOUBLE PRECISION Cbar4(3,3,3,3),Cref(3,3,3,3),Cspac(3,3,3,3),
     & TT1(3,3,3,3),TT2(3,3,3,3),TT3(3,3,3,3),TT4(3,3,3,3),
     & T41(3,3,3,3),T42(3,3,3,3),T43(3,3,3,3),T44(3,3,3,3),
     & ProjTtilda(3,3,3,3)
      INTEGER i,j,k,l,ic,jc,kc,lc,IO
c Form identity matrix
      do i=1,3
       do j=1,3
        Identity(i,j)=delta(i,j)
       end do
      end do
c Calculate CBar4
      aaa=2.0d0*alpha*gamma*
     & exp(gamma*(II-3.0d0))*JJ**(-4.0d0/3.0d0)
      call TensorProduct(CBar4,Identity,Identity,aaa)
c Calculate Cref
      call TensorProduct(TT1,Cinv,Cinv,-1.0d0/3.0d0)
      call WheelProduct(TT2,Cinv,1.0d0)
      call AddTens4(ProjTtilda,TT1,TT2)
      call TensorProduct(TT1,Cinv,Siso,-2.0d0/3.0d0)
      call TensorProduct(TT2,Siso,Cinv,-2.0d0/3.0d0)
      aaa=2.0d0/3.0d0*JJ**(-2.0d0/3.0d0)*DoubleDot(SBar,C)
      call ScalTens4(TT3,ProjTtilda,aaa)
      call AddTens4(TT4,TT1,TT2)
      call AddTens4(TT1,TT3,TT4)
      call T4ddT2(T21,CBar4,C,1.0d0)
      call TensorProduct(T41,Cinv,T21,-1.0d0/3.0d0)
      call TensorProduct(T42,T21,Cinv,-1.0d0/3.0d0)
      call AddTens4(T43,T41,T42)
      call T2ddT4(T22,C,CBar4,1.0d0)
      bbb=1.0d0/9.0d0*DoubleDot(T22,C)
      call TensorProduct(T44,Cinv,Cinv,bbb)
      call AddTens4(T42,T44,T43)
      call AddTens4(TT3,T42,CBar4)
      call AddTens4(Cref,TT1,TT3)
c Calculate spatial DEViatoric tangent moduli (push-forward)
      do i=1,3
        do j=1,3
          do k=1,3
            do l=1,3
              Cspac(i,j,k,l)=0.0d0
              do ic=1,3
                do jc=1,3
                  do kc=1,3
                    do lc=1,3
                      Cspac(i,j,k,l)=Cspac(i,j,k,l)+
     & F(i,ic)*F(j,jc)*F(k,kc)*F(l,lc)*
     & Cref(ic,jc,kc,lc)/JJ
                    end do
                  end do
                end do
              end do
            end do
```

```
          end do
        end do
      end do
      END
c ***********************************************************************
```

APPENDIX D

NOTATION

Notation adopted in this dissertation is not entirely orthodox and may require additional comments. Traditionally, in the English language scientific literature vectors are denoted by bold lowercase letters (i.e. $\boldsymbol{v}$), and tensors are denoted by bold capital letters (i.e. $\boldsymbol{A}$). No distinction is usually made between second-order and higher-order tensors. Further confusion is caused by the fact that certain tensors (i.e. Cauchy stress) are commonly denoted by a lower-case letter (i.e. $\boldsymbol{\sigma}$). In order to avoid confusion, as well as to satisfy his own aesthetic preferences, the author of this work uses notation more commonly found in Russian scientific texts. Thus in this manuscript, vectors are underlined (i.e. $\underline{v}$), second-order tensors are underlined twice (i.e. $\underline{\underline{A}}$), and for differentiating higher-order tensors from second-order tensors, a left superscript (denoting the order of the tensor) is utilized (i.e. ${}^{4}\underline{\underline{P}}$).

The following convention is adopted throughout the text for tensor operations:

:	inner product
·	scalar product
×	vector product
⊗	tensor product

BIBLIOGRAPHY

[1] Rinkel GJE, Djibuti M, Algra A, van Gijn J. Prevalence and risk of rupture of intracranial aneurysms: A systematic review. *Stroke* 1998; **29**, 1: 251-256.

[2] Newman AB, Arnold AM, Burke GL, O'Leary DH, Manolio TA. Cardiovascular disease and mortality in older adults with small abdominal aortic aneurysms detected by ultrasonography. *Ann Intern Med* 2001; **134**: 182-190.

[3] Quill DS, Colgan MP, Sumner DS. Ultrasonic screening for the detection of abdominal aortic aneurysms. *Surg Clin North Am* 1989; **69**: 713-720.

[4] McCombs RP, Roberts B. Acute renal failure after resection of abdominal aortic aneurysm. *Surg Gynecol Obstet* 1979; **148**: 175-179.

[5] Johnston KW. Multicenter prospective study of nonruptured abdominal aortic aneurysm; II: Variables predicting morbidity and mortality, *J Vasc Surg* 1989; **9**: 437-447.

[6] Hollier LH, Taylor LM, Ochsner J. Recommended indications for operative treatment of abdominal aortic aneurysms. *J Vasc Surg* 1992; **6**: 1046-1056.

[7] Humphrey JD. *Cardiovascular Solid Mechanics: Cells, Tissues, and Organs.* Springer: New York, 2002; 386.

[8] Holzapfel GA, Gasser TG, Ogden RW. A New Constitutive Framework for Arterial Wall Mechanics and a Comparative Study of Material Models. *J Elast* 2000; **61**: 1-48.

[9] Scott S, Ferguson GG, Roach MR. Comparison of the elastic properties of human intracranial arteries and aneurysms. *Canadian Journal of Physiology and Pharmacology* 1972; **50**: 328-332.

[10] Nyström SHM. Development of intracranial aneurysms as revealed by electron microscopy. *Neurosurgery* 1963; **20**: 329-337

[11] Drangova M, Holdsworth DW, Boyd CJ, Dunmore PJ, Roach MR, Fenster A. Elasticity and geometry measurements of vascular specimens using a high-resolution laboratory CT scanner. *Physiol Meas* 1993; **14**: 277-290

[12] Slaughter WS. *The Linearized Theory of Elasticity*. Birkhäuser: Boston, 2002; 267.

[13] Bellamy K, Limbert G, Watersa MG, Middleton J. An elastomeric material for facial prostheses: synthesis, experimental and numerical testing aspects. *Biomaterials* 2003; **24**: 5061–5066.

[14] Büchler P, Ramaniraka NA, Rakotomanana LR, Iannotti JP, Farron A. A finite element model of the shoulder: application to the comparison of normal and osteoarthritic joints. *Clinical Biomechanics* 2002; **17**: 630-639.

[15] Cheung JT, Zhang M, Leung AK, Fan Y. Three-dimensional finite element analysis of the foot during standing – a material sensitivity study. *Journal of Biomechanics* 2005; **38**: 1045-1054.

[16] ABAQUS Manual. Hibbitt, Karlsson and Sorensen: 1080 Main Street, Pawtucket, RI 02860, USA, 2003.

[17] Almeida ES, Spilker RL. Finite element formulations for hyperelastic transversely isotropic biphasic soft tissues. *Comput Methods Appl Mech Engrg* 1998; **151**: 513-538.

[18] ANSYS, Inc. Release 10.0 Theory Reference, Canonsburg, PA, USA: ANSYS Inc., 2005.

[19] Kaliske M. A Formulation of Elasticity and Viscoelasticity for Fibre Reinforced Material at Small and Finite Strains. *Comput Methods Appl Mech Engrg* 2000; **185**: 225-243.

[20] LS-DYNA Theoretical Manual, compiled by Hallquist JO, 2876 Waverly Way, Livermore, CA 94550-1740, USA: Livermore Software Technology Corporation, 1998.

[21] Weiss JA, Maker BN, Govindjee S. Finite element implementation of incompressible, transversely isotropic hyperelasticity. *Comput Methods Appl Mech Engrg*. 1996; **135**: 107-128

[22] Guccione JM, McCulloch AD, Waldman LK. Passive material properties of intact ventricular myocardium determined from a cylindrical model. *Journal of Biomechanical Engineering, Transactions of the ASME* 1991; **113**, 1: 42-55.

[23] Vawter DL. Finite Element Model for Macroscopic Deformation of the Lung. *Journal of Biomechanical Engineering, Transactions of the ASME* 1980; **102**, 1: 1-7.

[24] Humphrey JD, Rajagopal KR. A constrained mixture model for growth and remodeling of soft tissues. *Mathematical Models and Methods in Applied Sciences* 2002; **12**: 407-430

[25] Wulandana R, Robertson AM. An Inelastic Multi-Mechanism Constitutive Equation for Cerebral Arterial Tissue. *Biomechanics and Modeling in Mechanobiology* 2005; **4**: 235-248.

[26] Tobolsky A, Prettyman I, Dillon J. Stress relaxation of natural and synthetic rubber stocks. *Journal of Applied Physics* 1944; **15**: 380-395.

[27] Wulandana R. *A Nonlinear and Inelastic Constitutive Equation for Human Cerebral Arterial and Aneurysm Walls*, University of Pittsburgh: Pittsburgh, PA, 2003

[28] Carew TE, Ramesh NV, Patel DJ. Compressibility of the arterial wall, *Circ Res* 1968; **23**: 61-68.

[29] Boutouyrie P, Germain DP, Tropeano AI, Laloux B, Carenzi F, Zidi M, Jeunemaitre X, Laurent S. Compressibility of the Carotid Artery in Patients With Pseudoxanthoma Elasticum. *Hypertension* 2001; **38**: 1181-1184.

[30] Chuong CJ, Fung YC. Compressibility and constitutive equation of arterial wall in radial compression experiments. *J Biomech* 1984; **17**: 35-40.

[31] Simo JC, Hughes TJR. *Computational Inelasticity*. Springer: New York 1998; 348.

[32] Guide to ANSYS User Programmable Features, Canonsburg, PA, USA: ANSYS Inc., 2005.

[33] Taber's Cyclopedic Medical Dictionary (2001). Retrieved 14 November 2006, from xreferplus. http://xreferplus.com/entry/4787652.

[34] Hasso AN, Bird CR. Percutaneous Translumenal Angioplasty of Carotid and Vertebral Arteries. In: Jang GD, editor. Angioplasty. McGraw-Hill, 1986; 104-115.

[35] Holzapfel GA, Schulze–Bauer CAJ, Stadler M. Mechanics of Angioplasty: Wall, Balloon and Stent. In: *Mechanics in Biology*, edited by Casey J and Bao G, American Society of Mechanical Engineers: New York 2000; **46**: 141-156.

[36] Holzapfel GA, Stadler M, Schulze–Bauer CAJ. A Layer-Specific Three-Dimensional Model for the Simulation of Balloon Angioplasty using Magnetic Resonance Imaging and Mechanical Testing. *Annals of Biomedical Engineering* 2002; **30**: 753-767.

[37] Foutrakis GN, Yonas H, Sclabassi RJ. Saccular Aneurysm Formation in Curved and Bifurcating Arteries. *American Journal of Neuroradiology* 1999; **20**: 1309-1317.

[38] Tateshima S, Murayama Y, Villablanca JP, Morino T, Nomura K, Tanishita K, Viñuela F. In Vitro Measurement of Fluid-Induced Wall Shear Stress in Unruptured Cerebral Aneurysms Harboring Blebs. *Stroke* 2003; *34*: 187-192.

[39] Yasui T, Komiyama N, Nishikawa M, Nakajima H, Kobayashi Y, Inoue T. Fusiform vertebral artery aneurysms as a cause of dissecting aneurysms. *J Neurosurg* 1999; **91**: 139-144.

[40] Da Silva ES, Rodrigues AJ, de Tolosa EMC, Rodrigues CJ, do Prado JVB, Nakamoto JC. Morphology and diameter of infrarenal aortic aneurysms: a prospective autopsy study. *Cardiovascular Surgery* 2000; **7**: 526-532.

[41] Watton PN, Hill NA, Heil M. A mathematical model for the growth of the abdominal aortic aneurysm. *Biomechan Model Mechanobiol* 2004; **3**: 98-113.

[42] Holzapfel GA. *Nonlinear Solid Mechanics: A Continuum Approach for Engineering*, Wiley: New York, 2000; 228.